https://doi.org/10.5194/egusphere-2026-3522
Preprint. Discussion started: 26 June 2026


# Satellite-derived management indicators improve modeling of water and greenhouse gas fluxes in Swiss agroecosystems

Aolin Jia[1,2], Helge Aasen[2], Lukas Hörtnagl[1], Iris Feigenwinter[1], Sélène Ledain[2], Thomas Lauber[2], Kukka-Maaria Kohonen[1,3], Flavian Tschurr[1], Lorenz Allemann[1], Fabio Turco[1], and Nina Buchmann[1]

[1]Institute of Agricultural Sciences, Department of Environmental Systems Science, ETH Zürich, 8092 Zürich, Switzerland
[2]Earth Observation of Agroecosystems Team, Agroecology and Environment Division, Agroscope, 8046 Zürich, Switzerland
[3]Finnish Meteorological Institute, 00101 Helsinki, Finland

**Correspondence:** Aolin Jia (aolin.jia@usys.ethz.ch)

**Abstract.**

Agroecosystems regulate carbon, water, and nitrogen cycles, yet robust modeling of water and greenhouse gas (GHG) fluxes remains limited by incomplete or inaccessible information on field management practices. Although high-resolution remote sensing (RS) observations can detect management events such as mowing or harvest, their use for representing management intensity and associated impacts on ecosystem flux dynamics remains limited in existing models. Here, we developed an RS-assisted modeling framework to estimate daily latent heat flux (LE), net ecosystem $CO_2$ exchange (NEE), nitrous oxide ($N_2O$) and methane ($CH_4$) fluxes across six Swiss FluxNet sites (two croplands and four grasslands) between 2016 and 2025. Sentinel-2 time series were used to derive leaf area index and RS-based field management indices (RS-FMIs), detecting mowing events, quantifying defoliation intensity, and identifying crop rotation and bare soil periods. These indicators were combined with meteorological drivers to train XGBoost models for each ecosystem type and target variable separately, and driver contributions were evaluated using SHapley Additive exPlanations (SHAP) analysis.

The RS-FMIs effectively captured *in situ* recorded management events and enabled improved reconstruction of daily flux variability. Model performances were strong for LE ($R^2 \approx 0.89$–$0.90$) and NEE ($R^2 \approx 0.59$–$0.71$), whereas $N_2O$ and $CH_4$ fluxes were reproduced with moderate accuracy ($R^2 \approx 0.37$–$0.55$). Models using RS-FMIs performed similarly to those using well-compiled *in situ* management records, supporting the ability of RS-derived vegetation and management indicators to represent management effects. LE variability was primarily energy-driven and dominated by meteorological conditions, whereas vegetation dynamics and RS-FMIs played stronger roles in shaping NEE, $N_2O$, and $CH_4$ variability. These results demonstrate that RS-FMIs offer new opportunities to reconstruct management information and improve the representation of management effects in agroecosystem flux modeling.

## 1 Introduction

Agroecosystems contribute roughly one-fifth of global anthropogenic greenhouse gas (GHG) emissions and account for approximately seventy percent of global freshwater withdrawals, underscoring their central role in climate change, water scarcity, and food security (McDermid et al., 2023; Nabuurs et al., 2023; Tian et al., 2024; United Nations, 2020). Accurate quantifi-

https://doi.org/10.5194/egusphere-2026-3522
Preprint. Discussion started: 26 June 2026


cation of anthropogenic GHG fluxes—namely carbon dioxide ($CO_2$), nitrous oxide ($N_2O$), and methane ($CH_4$)—along with evapotranspiration (ET) is therefore essential for characterizing the atmospheric components of carbon, nitrogen, and water, as well as understanding agroecosystem responses to climate variability (Yang et al., 2024). In this context, Switzerland represents a heterogeneous agroecosystem landscape dominated by intensively managed grasslands and croplands (Pazúr et al., 2022). Common agricultural practices, such as crop rotation, fertilization, harvesting, and mowing in grasslands, exert strong and nonlinear influences on GHG emissions and water use by altering canopy phenology and performance, soil biogeochemistry, and surface energy–water exchange (Heimsch et al., 2024; Henne et al., 2016; Wang et al., 2026). However, land-use heterogeneity and limited availability of management information introduce substantial uncertainty in modeling GHG and ET dynamics (Nelson et al., 2024; Zentgraf et al., 2025).

Field studies have provided valuable insights into the drivers of agroecosystem GHG fluxes, demonstrating that management practices, vegetation dynamics, and meteorological forcing regulate GHG exchange (Emmel et al., 2018; Feigenwinter et al., 2023a; Hörtnagl et al., 2018; Maier et al., 2022; Merbold et al., 2014; Rogger et al., 2022). Vegetation is central to this regulation because it couples carbon, nitrogen, water, and energy exchanges through canopy structure, physiological activity, and surface–atmosphere interactions, while also shaping soil microenvironmental conditions that govern GHG emissions (Law et al., 2002). Long-term eddy-covariance (EC) observations indicate that mowing-induced disturbances can drive $CO_2$ source–sink shifts through abrupt defoliation and reduced photosynthetic capacity, with effects comparable to meteorological forcing (Feigenwinter et al., 2023b), while post-harvest bare soil periods in croplands are associated with strong but short-lived $N_2O$ emission pulses (Maier et al., 2025; Merbold et al., 2014). However, these insights are largely derived from site-level observations at locations with detailed management records, limiting their spatial representativeness across heterogeneous agricultural landscapes (Rebmann et al., 2018). To move beyond site-level observations, regional studies and modeling frameworks have been developed to characterize GHG flux dynamics. Process-based models (Smith et al., 2008), such as the Denitrification-Decomposition model (DNDC) or DayCENT, enable large-scale simulation of carbon and nitrogen fluxes, but their performance strongly depends on detailed input data, parameterization schemes, and site-specific calibration, particularly in agricultural systems where management information is often incomplete or inaccessible (Dietiker et al., 2010; Gaillard et al., 2018; Guo et al., 2023; Hastings et al., 2010; Mathers et al., 2023; Yue et al., 2019).

High-resolution remote sensing (RS) offers a promising pathway to address this gap by providing spatially explicit information on vegetation dynamics, phenology, and management disturbance signals that are closely linked to management activities and ecosystem flux responses (Aasen et al., 2018; Dusseux et al., 2014; Jia et al., 2025). Satellite time series have been used to identify the timing and frequency of mowing, crop harvest, and other defoliation events (e.g., grazing and tillage), yet less attention has been given to representing disturbance magnitude and post-disturbance recovery dynamics in forms directly relevant to ecosystem flux responses (Andreatta et al., 2022; De Vroey et al., 2022; Reinermann et al., 2020; Schwieder et al., 2022; Zhou et al., 2021). Beyond detecting management events, RS enables the monitoring of vegetation structural states and fractional cover that regulate GHG fluxes across scales (Gottschalk et al., 2024). However, this information remains underutilized in many current flux modeling frameworks (Yang et al., 2023a; Yuan et al., 2009), particularly for non-$CO_2$ fluxes (Ivanova et al., 2026). In comparison, RS is widely used for regional ET estimation through energy-balance and machine-learning ap-

https://doi.org/10.5194/egusphere-2026-3522
Preprint. Discussion started: 26 June 2026


proaches, yet management-induced disturbances are rarely explicitly represented in such frameworks (Chen and Liu, 2020; Jia et al., 2026). Integrating RS-derived indicators of management and vegetation dynamics, therefore, offers new opportunities to improve flux modeling and to disentangle the relative contributions of management, vegetation, and meteorological forcing (Nelson et al., 2024; Yang et al., 2023b).

Consequently, this study examines whether incorporating high-resolution, satellite-derived management and vegetation indicators can enhance the simulation and driver attribution of latent heat flux (LE), NEE, $N_2O$, and $CH_4$ fluxes across Swiss grassland and cropland agroecosystems. To address this question, we

(1) derive management indicators by detecting management events and quantifying management intensity from high-resolution RS observations;
(2) compare RS-derived management indicators with site management records to evaluate their consistency;
(3) test whether RS-based indicators of management and vegetation state provide relevant information complementary to meteorological forcing for flux modeling; and
(4) quantify flux sensitivity to management, vegetation structural and functional indicators, and meteorological drivers.

While spatial upscaling to unobserved regions remains outside the scope of this work, this study provides a targeted, site-level evaluation designed to unlock the complementary value of RS indicators for capturing daily flux dynamics within established monitoring networks.

## 2 Data and Methods

### 2.1 Data

#### 2.1.1 Swiss FluxNet

The Swiss FluxNet is the national eddy-covariance (EC) network that quantifies ecosystem–atmosphere exchange of $CO_2$, $N_2O$, and $CH_4$, as well as water vapor fluxes, across major land-use types and climatic gradients (Buchmann et al., 2019). The network integrates long-term ecosystem flux measurement sites that quantify turbulent fluxes of $CO_2$ and $H_2O$ at 20 Hz with the EC method and aggregate fluxes to half-hourly resolution (Baldocchi et al., 1988). In addition, at selected sites, $CH_4$ and $N_2O$ fluxes were observed at 10 Hz to capture trace gas dynamics in managed agroecosystems. In this study, six agricultural sites were selected (Table 1), including croplands and grasslands spanning a wide elevation range, from intensively and moderately managed grasslands in the lowlands to high-elevation grasslands (Figure 1). Each site is equipped with standardized micrometeorological instrumentation to measure ecosystem fluxes and meteorological variables following international EC protocols (Eugster and Merbold, 2015). Site management activities are systematically recorded by category together with their corresponding dates. Data processing includes quality control, coordinate rotation, and frequency response correction, procedures consistent with community standards that enable cross-site comparability and long-term consistency (Hörtnagl et al., 2025; Sabbatini et al., 2018). The Swiss FluxNet provides harmonized flux and meteorological datasets to international research infrastructures, including the Integrated Carbon Observation System (ICOS) (Heiskanen et al., 2022) and FLUXNET

https://doi.org/10.5194/egusphere-2026-3522
Preprint. Discussion started: 26 June 2026


(Baldocchi et al., 2001), enabling the integration of Swiss ecosystem observations into continental and global assessments of GHG and water fluxes.

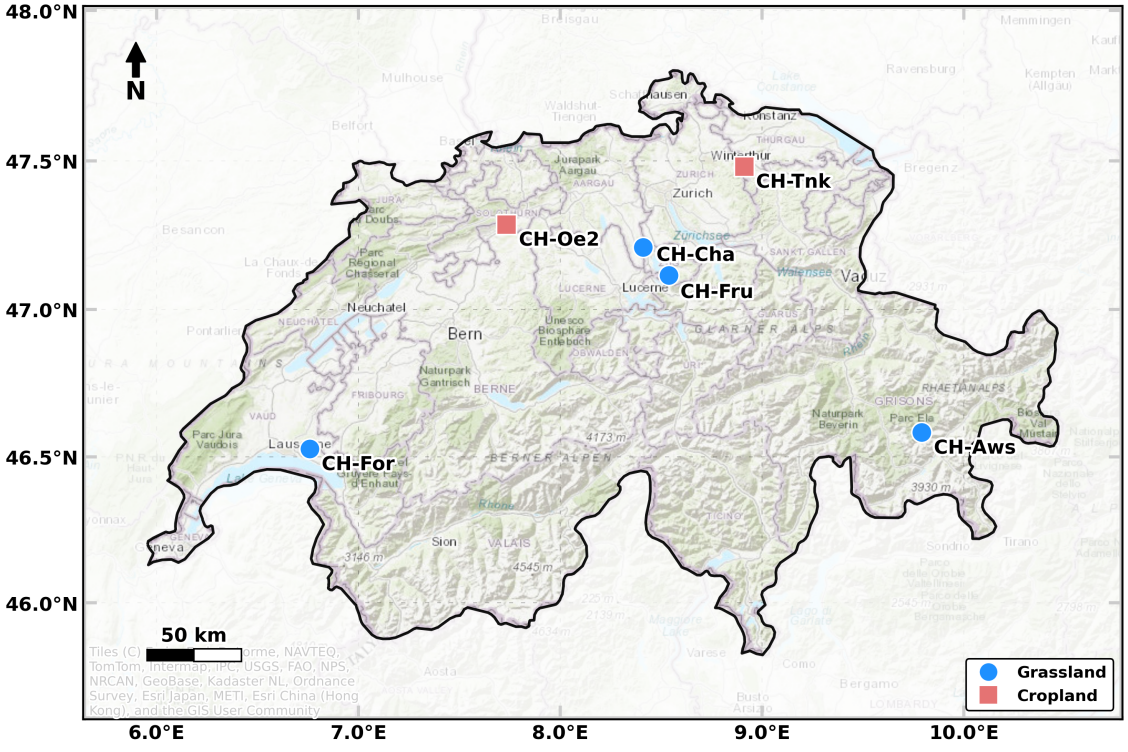


**Figure 1.** Map of the Swiss FluxNet sites used in this study, with blue circles indicating grasslands and red squares indicating croplands. Forel (CH-For), despite being a cropland, was a temporary grassland at the time of the study while the others are either permanent grasslands or croplands. Basemap sources: Esri, DeLorme, NAVTEQ, TomTom, Intermap, iPC, USGS, FAO, NPS, NRCAN, GeoBase, Kadaster NL, Ordnance Survey, Esri Japan, METI, Esri China (Hong Kong), and the GIS User Community | Powered by Esri.

**Table 1.** Metadata of Swiss FluxNet sites used in this study. Forel (CH-For) was a temporary grassland within a crop rotation at the time of the study while the others are permanent grasslands (CH-Cha, CH-Fru, CH-Aws) or croplands (CH-Oe2, CH-Tnk).

| Site ID | Site name | Latitude | Longitude | Ecosystem type | Elevation (m) | Selected period | Flux Variables | Data Source |
|---|---|---|---|---|---|---|---|---|
| CH-Cha | Chamau | 47.210222 | 8.410444 | Grassland | 393 | 2016–2024 | LE, NEE, $N_2O$, $CH_4$ | Hörtnagl et al. (2025) |
| CH-Fru | Früebüel | 47.115833 | 8.537778 | Grassland | 982 | 2016–2024 | LE, NEE | Buchmann et al. (2025) |
| CH-Aws | Alp Weissenstein | 46.583102 | 9.790624 | Grassland | 1978 | 2016–2024 | LE, NEE | Buchmann et al. (2026a) |
| CH-For | Forel | 46.527194 | 6.759528 | Grassland | 752 | 2024–2025 | LE, NEE, $N_2O$, $CH_4$ | In preparation |
| CH-Oe2 | Oensingen | 47.286417 | 7.733750 | Cropland | 452 | 2016–2024 | LE, NEE, $N_2O$, $CH_4$ | Buchmann et al. (2026b) |
| CH-Tnk | Tänikon | 47.480620 | 8.911868 | Cropland | 547 | 2023–2025 | LE, NEE, $N_2O$, $CH_4$ | Turco et al. (2025) |

https://doi.org/10.5194/egusphere-2026-3522
Preprint. Discussion started: 26 June 2026


*In situ* meteorological measurements, EC flux data, and recorded management information were used in this study. LE, NEE, $N_2O$, and $CH_4$ fluxes were defined as target variables, while meteorological and management variables served as driving factors. No surface energy balance closure correction was applied to LE flux. Management records were represented as the number of days since mowing (TIME_SINCE_MOW), grazing (TIME_SINCE_GRAZ), harvest (TIME_SINCE_HARV), soil cultivation (TIME_SINCE_SCULT), and fertilization (TIME_SINCE_FERT). Converting discrete management events into continuous temporal metrics has been shown to be a practical approach for diagnosing variability in GHG fluxes within data-driven modeling frameworks (Feigenwinter et al., 2023a, b; Gnisia et al., 2025; Wang et al., 2026). Values greater than 30 days were capped at 30, based on the assumption that management disturbance effects become negligible beyond approximately one month and to prevent the model from interpreting these features as a proxy for day of year (Phillips et al., 2009). Fertilization amount was not included due to its limited availability and associated record uncertainty across sites.

The published half-hourly data were quality-controlled, with gaps filled using Random Forest and accompanied by associated flags (Feigenwinter et al., 2023a). Air temperature (Ta), precipitation (P), solar radiation (Rg), and vapor pressure deficit (VPD) were selected as key meteorological factors. All drivers and flux variables were aggregated to daily means, except P, which was aggregated to daily sums. Days were excluded when more than 50% of half-hourly records were gap-filled; otherwise, daily meteorological and flux means were computed using both measured and gap-filled records. Retaining gap-filled records in the daily aggregation helped mitigate aggregation biases for variables with strong diurnal variability. To identify satellite pixels contributing to site-level flux variability, the source area of the *in situ* half-hourly EC measurements was estimated using a flux footprint model (Kljun et al., 2015), and daily footprints were then derived by averaging the half-hourly footprints weighted by the absolute magnitude of the target flux. Pixels covering 90% of the cumulative footprint contribution were considered.

Meteorological temporal features were included to represent short- and long-term lag effects. Daily Ta and P over the preceding week (e.g., Ta-1d denotes the daily mean Ta on the previous day) were included to capture short-term lag effects, while rolling means of Ta and cumulative P over the preceding 15 and 30 days were used to represent longer-term memory effects. This study aims to evaluate potential drivers that could support future regional upscaling of LE and GHG fluxes, while the present analysis remains restricted to site-level model evaluation within the Swiss FluxNet network. Due to the limited availability of gridded soil moisture and soil temperature data, these variables were not included in the analysis. Precipitation-based temporal features partially capture moisture variability. To ensure consistency with satellite observations, only *in situ* data from 2016 onward were included in the analysis.

### 2.1.2 Sentinel-2 Satellite Products

Sentinel-2 surface reflectance data were used to characterize vegetation dynamics and surface conditions at high spatial resolution. We employed atmospherically corrected Level-2 products from the MultiSpectral Instrument (MSI), which provide observations in visible, near-infrared, and shortwave infrared bands at 10–20 m spatial resolution with an approximate 5-day revisit frequency (Liang et al., 2024; Richter et al., 2012). Snow-covered and cloudy pixels were removed based on quality flags and scene classification layers.

https://doi.org/10.5194/egusphere-2026-3522
Preprint. Discussion started: 26 June 2026


Fractional vegetation cover (FVC) was estimated based on spectral mixture analysis, in which the satellite surface reflectance signal is modeled as a linear combination of photosynthetic vegetation (PV), non-photosynthetic vegetation (NPV), and bare soil. Machine learning–based spectral unmixing models were trained to predict the fractional covers of these three components. We followed the methodology proposed by Lobert et al. (2025). Pure green and brown vegetation spectra were sampled from Sentinel-2 imagery acquired over Swiss croplands and grasslands between 2021 and 2023. Soil spectra were derived from a five-year Sentinel-2 bare soil reflectance composite (SoilSuite) developed by the German Aerospace Center (Karlshoefer et al., 2025). Within Swiss arable land, soil spectra were clustered into five groups using K-means to capture representative variability across the country. These pure endmember spectra were linearly mixed to generate synthetic training data (Okujeni et al., 2013). For each cover type (PV, NPV, and soil), an ensemble of five neural network models was trained on the synthetic mixtures to predict fractional cover. Evaluation on independent synthetic test sets yielded root mean squared errors (RMSEs) of 0.08 for PV and NPV fraction predictions and 0.05 for soil fraction prediction. The vegetation products were linearly interpolated over time.

Leaf area index (LAI) was retrieved from Sentinel-2 imagery using a specifically trained neural network (NN). The approach follows the development of operational global LAI products (Weiss and Baret, 2016), with adaptations to Swiss vegetation and soil conditions. Training data were generated using the PROSAIL radiative transfer model (Jacquemoud et al., 2009) to simulate Sentinel-2 canopy reflectances as a function of leaf biophysical parameters and canopy structural characteristics, including LAI. Model parameters were configured to represent typical crop types and grasslands in Switzerland (Atzberger et al., 2015; Graf et al., 2023). To better characterize canopy background effects, particularly under low LAI conditions when soil contributions to reflectance are more pronounced, soil spectra derived from Sentinel-2 imagery across Switzerland were incorporated into the PROSAIL simulations. LAI was subsequently used as a remote sensing–based vegetation performance index (RS-VPI) in the flux modeling framework.

Crop type maps were produced following Turkoglu et al. (2025, 2021) from Sentinel-2 time series imagery using a U-Net Temporal Attention Encoder (U-TAE; Sainte Fare Garnot and Landrieu, 2022), a deep learning architecture designed for multi-temporal satellite image segmentation. The model leverages temporal self-attention to dynamically weight observations across the growing season, enabling it to capture vegetation performance trajectories characteristic of different crop types. Because climate variability can shift the timing of growth stages substantially across years, observations were re-indexed by thermal time, warping the time axis so that equivalent vegetation stages are more consistently aligned across seasons (Turkoglu et al., 2025). In short, training was performed on parcel-level reference data from the Swiss agricultural compensation database provided by the Swiss Federal Office for Agriculture (Bundesamt für Landwirtschaft (BLW), 2024), which provides annually updated crop declarations across Switzerland. The model was evaluated on a held-out year and achieved an overall accuracy of 75%, an intersection over union (IoU) of 61%, and a mean IoU (mIoU) of 42%. Overall accuracy reflects the fraction of pixels correctly classified; IoU measures the overlap between predicted and ground-truth areas relative to their union; and mIoU averages this metric across all crop classes, giving equal weight to rare and common classes alike. Crop type data were used for two applications, first to identify neighboring pixels with the same vegetation types for the calculation of defoliation intensity (Section 2.2.3) and second to represent crop rotations, with both being treated as RS-based field management indices

https://doi.org/10.5194/egusphere-2026-3522
Preprint. Discussion started: 26 June 2026


(RS-FMIs). Crop type was first assigned to each day based on the nearest classification result and then converted into numerical model inputs using one-hot encoding, where each crop class was represented by a separate 0/1 variable indicating whether that crop type occurred on that day.

## 2.2 Methods

### 2.2.1 Overall Framework

RS–based field management indicators (RS-FMIs) and LAI were integrated with meteorological drivers (METEO) to construct multiple modeling scenarios (Figure 2). We included two benchmark scenarios: a METEO-only baseline (Scenario 1) and an *in situ* management-informed configuration combining METEO with site management (MGMT) records (Scenario 4).

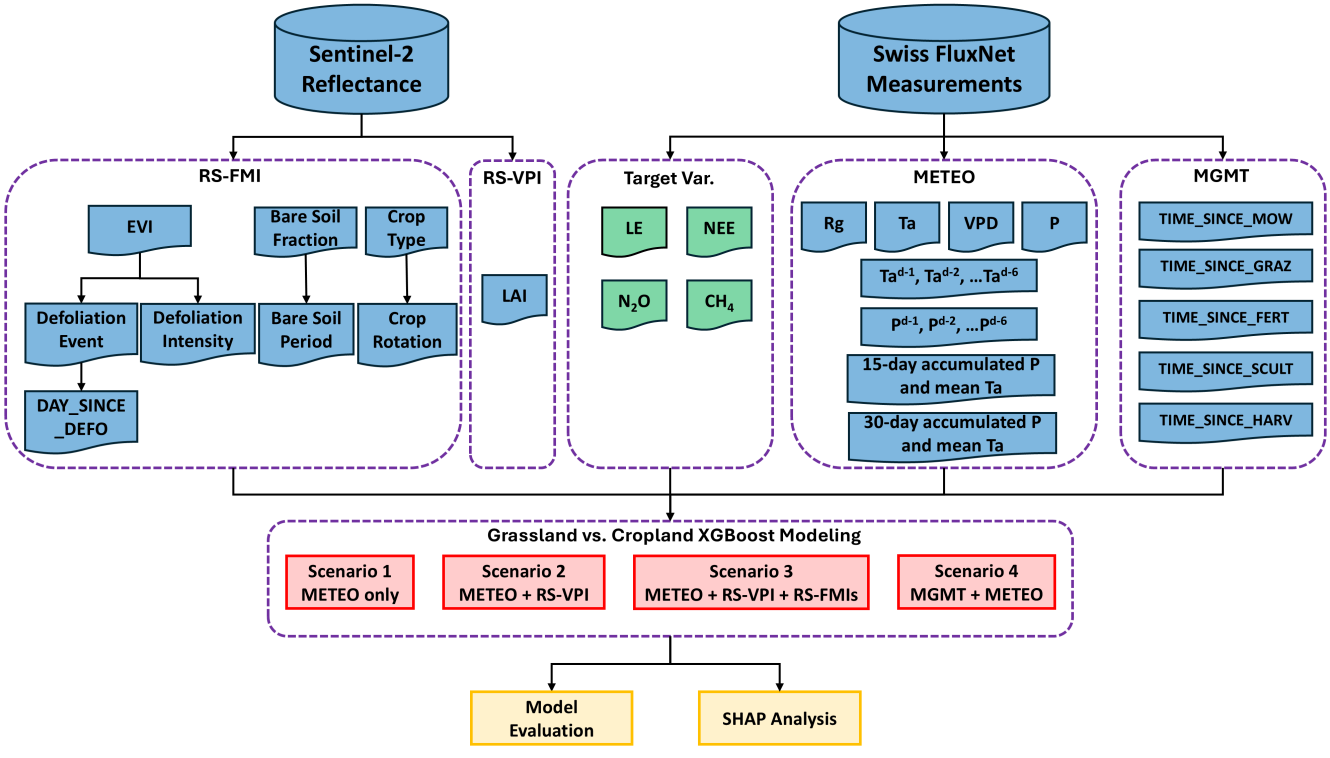


**Figure 2.** Overall methodological framework of this study, combining satellite products and *in situ* measurements. The target variables modeled at the daily scale include latent heat (LE), net ecosystem $CO_2$ exchange (NEE), nitrous oxide ($N_2O$), and methane ($CH_4$) fluxes. The driving variables were grouped into four categories: remote sensing–based field management indices (RS-FMIs), remote sensing–based vegetation performance indicator (RS-VPI), meteorological variables (METEO; including precipitation (P), air temperature (Ta), vapor pressure deficit (VPD), and solar radiation (Rg)), and site management records (MGMT). Grasslands and croplands were modeled separately.

The framework was designed not only to evaluate model performance but also to attribute flux variability to specific driver groups. Model comparison quantified the incremental contribution of management information beyond meteorological forcing,

https://doi.org/10.5194/egusphere-2026-3522
Preprint. Discussion started: 26 June 2026


while SHapley Additive exPlanations (SHAP) analysis (Lundberg and Lee, 2017) was used to assess the relative importance of individual drivers. This dual approach enabled both performance-based evaluation and interpretation of driver effects across agroecosystems.

#### 2.2.2 Remotely-Sensed Defoliation Event Detection

Discrete management-related defoliation events (i.e., mowing, grazing, and harvest) were identified for each site from Sentinel-2 Enhanced Vegetation Index (EVI) time series using the rule-based phenology residual framework of Schwieder et al. (2022), applied pixel-wise for each year. The procedure consisted of three main steps: (1) construction of an undisturbed vegetation performance baseline by identifying up to five local EVI maxima within the growing season and linearly interpolating an upper-envelope curve between these vertices; (2) candidate event detection by jointly evaluating (i) the negative residual between observed EVI and the envelope, and (ii) the abrupt drop between two consecutive valid observations ($\Delta$Y), for which both criteria were assessed with pixel-wise adaptive thresholds; and (3) ecological and temporal consistency filtering by enforcing a minimum separation of >15 days between events, and excluding cloud-contamination artifacts characterized by unrealistically rapid recovery ($\Delta Y > 0.15$ within 5 days). This framework has been successfully applied in Switzerland (Weber et al., 2024), and we adopted the same parameter settings. At CH-Cha, the EVI-based defoliation detection showed good consistency with recorded mowing events while remaining less sensitive to subtle mowing/grazing signals (Appendix A). Based on remotely-sensed defoliation detection, discrete events were converted into the number of days since the last defoliation event (Days since Defoliation) and used as an RS-FMI driving factor for modeling.

#### 2.2.3 Remotely-Sensed Defoliation Intensity Estimation

Management records at flux sites typically report the timing of discrete events (e.g., mowing or harvest) but rarely quantify the magnitude of biomass removal or the subsequent vegetation recovery trajectory, with the Swiss FluxNet being an exception. Although high-resolution RS time series have proven effective for detecting the timing of such management-related disturbances, their potential to characterize disturbance intensity remains less explored. To address this limitation, we developed a Defoliation Intensity Index (DII) that quantifies the magnitude of vegetation disturbance relative to the surrounding vegetation performance background.

The DII is based on two assumptions. First, the temporal dynamics of site-level EVI reflect the combined influence of natural phenology and management disturbances. Second, because management activities are spatially localized within the tower footprint, the median EVI computed over a surrounding window of the same land cover type primarily captures background vegetation performance dynamics under the same meteorological conditions and is less affected by individual field operations. Deviations of the site-level EVI from this background signal therefore provide a proxy for disturbance intensity associated with defoliation events at any given site. Accordingly, DII (Eq. 1) is defined as

$$\mathrm{DII}(d) = \frac{\overline{\mathrm{EVI}}_{\mathrm{win}}(d) - \mathrm{EVI}_s(d)}{\sigma_{\mathrm{win}}(d)} \tag{1}$$

https://doi.org/10.5194/egusphere-2026-3522
Preprint. Discussion started: 26 June 2026


where $\overline{\mathrm{EVI}}_{\mathrm{win}}(d)$ denotes the median EVI on day $d$ within the spatial window surrounding any given site, $\mathrm{EVI}_s(d)$ represents the EVI at the flux site on day $d$, and $\sigma_{\mathrm{win}}(d)$ is the corresponding spatial standard deviation.

To reduce the influence of concurrent disturbances in surrounding pixels, $\overline{\mathrm{EVI}}_{\mathrm{win}}(d)$ and $\sigma_{\mathrm{win}}(d)$ were computed using only the upper 50% of EVI values within the spatial window. This filtering step was intended to reduce the influence of recently defoliated surrounding fields and to provide a more reasonable estimate of background vegetation performance, rather than to guarantee that the reference pixels were entirely undisturbed. Positive DII values indicate that the site EVI is substantially lower than the surrounding background vegetation state, suggesting recent biomass removal or strong disturbance, whereas values near zero indicate vegetation conditions comparable to the surrounding landscape. Following a defoliation event, vegetation regrowth gradually reduces the difference between site-level EVI and the surrounding background, leading to a progressive decline in DII over time. To account for differences in field size and spatial extent of management practices between agroecosystem types, the spatial window used to compute background EVI was determined separately for grasslands and croplands. Sensitivity analysis indicated that a 1 km window best captured management-related disturbance signals in grasslands, whereas a 2 km window was more appropriate for croplands (Appendix B). These window sizes were therefore adopted to derive the final DII time series used in subsequent modeling analyses. The rate at which DII declines after a disturbance may also partly reflect fertilization conditions, because nutrient inputs can accelerate post-disturbance vegetation regrowth. This is particularly relevant for grassland sites, where fertilization often follows mowing. Importantly, DII does not represent a direct measurement of harvested biomass. Instead, it serves as a relative RS-derived proxy that characterizes the magnitude of vegetation deviations from the local vegetation performance background. By normalizing the EVI anomaly using the spatial variability within the spatial window, the index reduces sensitivity to absolute vegetation performance levels and allows more consistent identification of disturbance intensity across sites and seasons.

#### 2.2.4 Remotely-Sensed Bare Soil Period

Bare soil periods were identified from Sentinel-2 fractional vegetation model predictions to represent management-driven phases of canopy absence. In cropland systems, the presence and duration of bare soil are largely determined by post-harvest management decisions, such as whether cover crops are established, residues are retained, or soils are tilled (Poeplau and Don, 2015). Therefore, bare soil periods serve as an indicator of management strategy rather than merely a surface condition. A field was classified as bare when the bare soil fraction exceeded 0.5. Consecutive days meeting this criterion were grouped into a continuous bare soil period. The duration of bare conditions was quantified as the number of days since the onset of the bare soil period.

#### 2.2.5 Modeling Configuration

To estimate daily fluxes of LE, NEE, $N_2O$, and $CH_4$, we developed a tree-ensemble regression framework based on XGBoost (Chen and Guestrin, 2016). For each target variable, models were trained using daily samples pooled across all sites within a given agroecosystem category (cropland or grassland). To reduce overfitting while retaining samples from all sites, samples were randomly split into training (80%) and validation (20%) subsets for cross-scenario performance evaluation. In addition,

https://doi.org/10.5194/egusphere-2026-3522
Preprint. Discussion started: 26 June 2026


data from 2021 were excluded from model training and reserved as an independent time-series evaluation set. This evaluation design assessed the informational value of RS-derived drivers within the Swiss FluxNet site network and did not constitute an evaluation of spatial generalization to unmonitored locations.

Driving factors used as model predictors included (i) *in situ* meteorological (METEO) variables (Rg, VPD, Ta, and P), incorporating short-term daily lags within one week and monthly aggregates to represent memory effects (Section 2.1.1); (ii) management (MGMT) reported by farmers expressed as continuous time-since-disturbance metrics (i.e., days since harvest, fertilization, and soil cultivation); (iii) remotely-sensed vegetation performance indicator (RS-VPI); and (iv) remotely-sensed field management indicators (RS-FMIs). Model performance was evaluated on the independent prediction subsets using $R^2$, RMSE, and bias. Bias is defined as the mean difference between modeled and reference measurements.

To systematically assess the relative contribution of information streams, we constructed four modeling scenarios (Figure 2): (1) METEO only; (2) METEO + RS-VPI; (3) METEO + RS-VPI + RS-FMIs; and (4) METEO + MGMT. This scenario design allowed quantification of the incremental contribution of management and remote sensing information beyond baseline meteorological forcing (Zhu et al., 2023). Each scenario was trained separately for every target variable, allowing flux-specific driver sensitivity analysis. By comparing predictive skill and error structures across scenarios and flux types, we quantified how RS-derived management signals and vegetation state modulate GHG and water exchange processes. Grassland and cropland systems were modeled separately to enable a comparison of their sensitivities to environmental and management drivers within a unified modeling framework. Previous work (Jung et al., 2020; Nelson et al., 2024; Tramontana et al., 2015) suggested that, in similar environmental prediction settings, differences in model performance were driven more by driver selection than by choice of tree-based algorithms. Accordingly, we prioritized a systematic evaluation of different driver information streams within a single ensemble modeling framework to isolate the contribution of each driver group.

Hyperparameter tuning was conducted independently for each target variable and modeling scenario within the training pool. Instead of exhaustive or randomized search strategies, we employed a predefined set of 10 parameter configurations designed to span a structured range from strongly regularized (shallow trees, high penalization, low flexibility) to highly flexible settings (deeper trees, weaker regularization). This design was intended to capture the dominant model behavior regimes while maintaining computational efficiency. This strict-to-loose grid was designed to systematically explore the bias–variance spectrum and balance model complexity against generalization performance. Each configuration was evaluated using repeated cross-validation (10 folds × 5 repeats), resulting in 50 validation folds per configuration. Within each repeat, 10% of the training pool was used for testing in each fold. Repeating the cross-validation procedure with different random splits ensures that hyperparameter selection was not sensitive to a single data partition and yielded a more stable estimate of generalization performance. The optimal configuration was selected by maximizing the difference between the mean and half standard deviation of cross-validated $R^2$, thereby favoring models with strong average performance and stable behavior across folds (Ying et al., 2025). Final models were retrained on the full training pool using the selected configuration and evaluated on the 20% independent validation subset. This strategy ensured that all reported results reflect optimally tuned, flux-specific models with controlled bias–variance trade-offs across scenarios. Exploratory tests with expanded search ranges did not yield consistent performance improvements. The final parameter configurations for each target variable are summarized in Appendix C.

https://doi.org/10.5194/egusphere-2026-3522
Preprint. Discussion started: 26 June 2026


#### 2.2.6 Driver Analysis

To quantify the relative contribution of individual variables to flux variability, a driver analysis was conducted using SHAP values derived from the optimized XGBoost models (Lundberg and Lee, 2017). Conditional SHAP provides a mathematically consistent attribution framework that decomposes model predictions into additive driver contributions. Unlike traditional importance metrics, this conditional SHAP approach accounts for the complex, non-linear interactions and multi-collinearity inherent in tree-ensemble models, offering a more robust interpretation of driver influence.

The analysis was performed for each target variable (LE, NEE, $N_2O$, $CH_4$) under the METEO + RS-VPI + RS-FMIs scenario to quantify the role of RS-derived indicators in explaining variations in LE and GHG fluxes. For each flux, SHAP values were computed using the TreeExplainer implementation, applied to the final tuned model trained on the full training pool. A positive SHAP value represents a positive effect on the predicted response variable (here: fluxes) compared to the overall mean (here: fluxes of one agroecosystem type), and vice versa for negative SHAP values. To ensure computational efficiency while preserving representativeness, SHAP evaluation was conducted on a random subsample (3000 samples) drawn from the training dataset. Feature (i.e., driver) importance was quantified using the mean absolute SHAP value for each driving variable, representing its average marginal contribution to model output magnitude across samples. Drivers were subsequently ranked according to their mean absolute SHAP values. This ranking reflects the relative explanatory importance of individual drivers drawn from METEO, RS-VPI, and RS-FMIs. Differences in driving factor ranking between grassland and cropland systems were used to characterize how dominant controls on water and GHG fluxes vary between the two agroecosystems. To further quantify the relative contribution of different driver categories, individual predictors were grouped based on their classes: METEO, RS-VPI, and RS-FMIs. For each category, absolute SHAP values were aggregated by summing the mean absolute SHAP values of all variables within the group. The resulting category-level contributions were then normalized by the total SHAP magnitude across all drivers, yielding relative contributions that sum to one for each flux and agroecosystem. This aggregation enabled a direct comparison of the relative importance of meteorological, vegetation, and management-related drivers across fluxes and between grassland and cropland systems.

## 3 Results

### 3.1 Evaluation of Remotely-sensed Defoliation Intensity Index

The remotely-sensed DII was evaluated against recorded management events at representative long-term grassland and cropland sites before being used as an RS-FMI in the flux modeling framework. At the CH-Cha grassland site, DII peaks generally coincided with recorded defoliation-related management events, including mowing, grazing, soil cultivation, and the grassland renewal event in 2021 (Figure 3a). The renewal event produced the strongest DII response, consistent with the severe vegetation disturbance caused by sward destruction and reseeding. Mowing and grazing events showed more variable DII amplitudes, indicating that DII captured differences in relative disturbance magnitude rather than merely recording event occurrence. Follow-

https://doi.org/10.5194/egusphere-2026-3522
Preprint. Discussion started: 26 June 2026


ing defoliation, DII generally declined over time, reflecting vegetation recovery toward the surrounding background vegetation state.

At the CH-Oe2 cropland site, DII also responded to harvest and soil cultivation events, with pronounced peaks during periods of abrupt canopy removal or surface disturbance (Figure 3b). Compared with grasslands, cropland DII dynamics were more strongly shaped by crop-specific phenological development and post-harvest bare soil phases. Nevertheless, the temporal correspondence between DII peaks and recorded management events indicates that the index captured major defoliation and disturbance signals across both agroecosystem types.

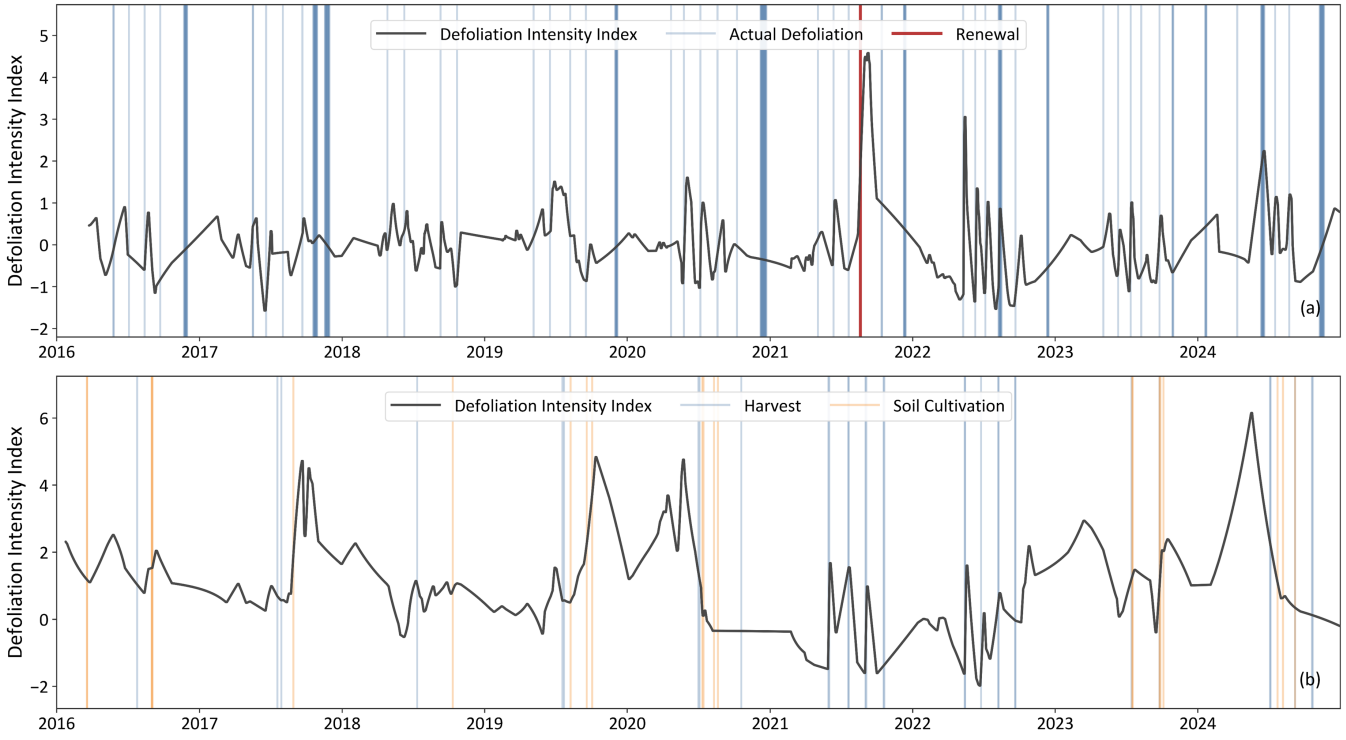


**Figure 3.** Evaluation of the remotely-sensed Defoliation Intensity Index (DII) at representative (a) grassland (CH-Cha) and (b) cropland (CH-Oe2) sites. Vertical lines indicate recorded management events, including mowing, grazing, renewal, and soil cultivation at the grassland site, and harvest and soil cultivation at the cropland site. DII peaks indicate periods when site-level EVI was substantially lower than the surrounding same-land-cover background, reflecting relative vegetation disturbance intensity.

Event-level comparisons with recorded yield further supported the interpretation of DII as a proxy for relative defoliation intensity (Figure 4). At the CH-Cha grassland site, the maximum DII around recorded defoliation events increased with harvested biomass ($r = 0.41$, $p = 0.003$), indicating that larger biomass removal generally produced stronger negative deviations of site-level EVI from the surrounding same-land-cover background. At the CH-Oe2 cropland site, DII showed a similar positive tendency with recorded yield, but the relationship was not statistically significant ($r = 0.36$, $p = 0.161$). This weaker

https://doi.org/10.5194/egusphere-2026-3522
Preprint. Discussion started: 26 June 2026


correspondence is consistent with the stronger influence of crop rotation, where the same recorded yield amount may produce different EVI responses depending on crop type, harvested component, and post-harvest surface conditions.

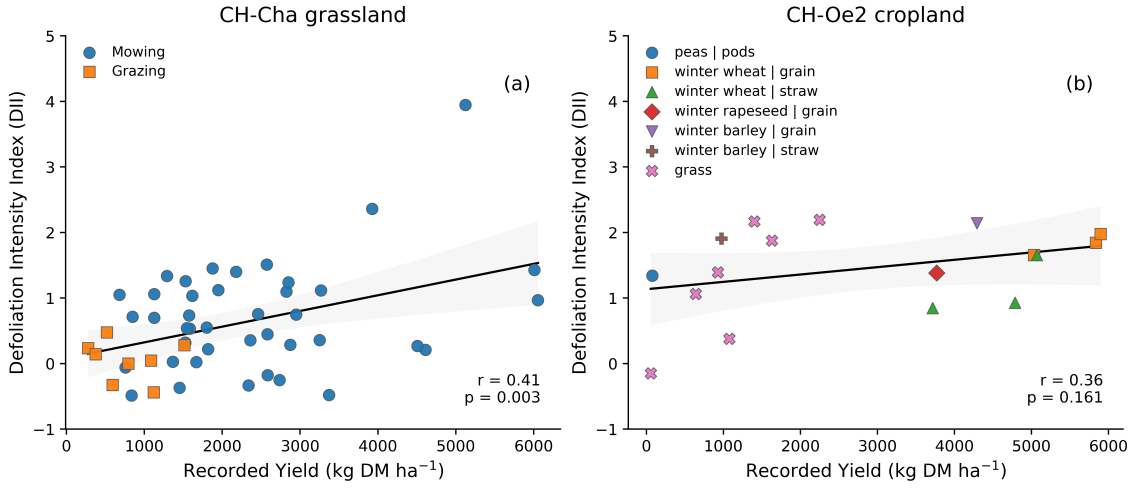


**Figure 4.** Relationship between recorded harvested dry matter (DM) and the maximum remotely-sensed Defoliation Intensity Index (DII) around recorded defoliation or harvest events at (a) CH-Cha grassland and (b) CH-Oe2 cropland. Points distinguish management or crop-specific harvest categories. The black line and shaded area show the linear fit and 95% confidence interval. Correlation statistics are shown for the event-level comparison.

Overall, these results showed that DII provided a continuous, remotely-sensed proxy for relative vegetation disturbance intensity and post-disturbance recovery dynamics. Unlike binary event indicators, DII preserved information on the magnitude and persistence of management-related canopy deviation from the local vegetation background, supporting its use as an RS-FMI in subsequent flux modeling analyses.

### 3.2 Model Evaluation

Model performance was evaluated using an independent validation sample group for four flux variables (LE, NEE, $N_2O$, and $CH_4$) under four scenarios (Figure 5).

In grasslands, LE was reproduced well across all scenarios, with consistently high performance ($R^2 = 0.87$–$0.89$; RMSE = 14.36–15.25 W m$^{-2}$; Figure 5a–d). Adding RS-derived vegetation performance indicators (RS-VPI) and management indices (RS-FMIs) resulted in only marginal changes relative to the METEO-only scenario. A slight saturation pattern was evident at high LE values, indicating a tendency to underestimate peak fluxes. NEE model performance was more sensitive to predictor choice than for LE (Figure 5e–h). The METEO-only scenario yielded the lowest skill ($R^2 = 0.45$; RMSE = 1.94 $\mu$mol $CO_2$ m$^{-2}$ s$^{-1}$), whereas the METEO + MGMT benchmark scenario increased $R^2$ to 0.58. Adding RS-derived vegetation performance indicators (RS-VPI) improved model performance relative to the METEO-only scenario ($R^2 = 0.55$ vs. 0.45). The additional inclusion of RS-derived management indices (RS-FMIs) resulted in a further but smaller improvement

https://doi.org/10.5194/egusphere-2026-3522
Preprint. Discussion started: 26 June 2026


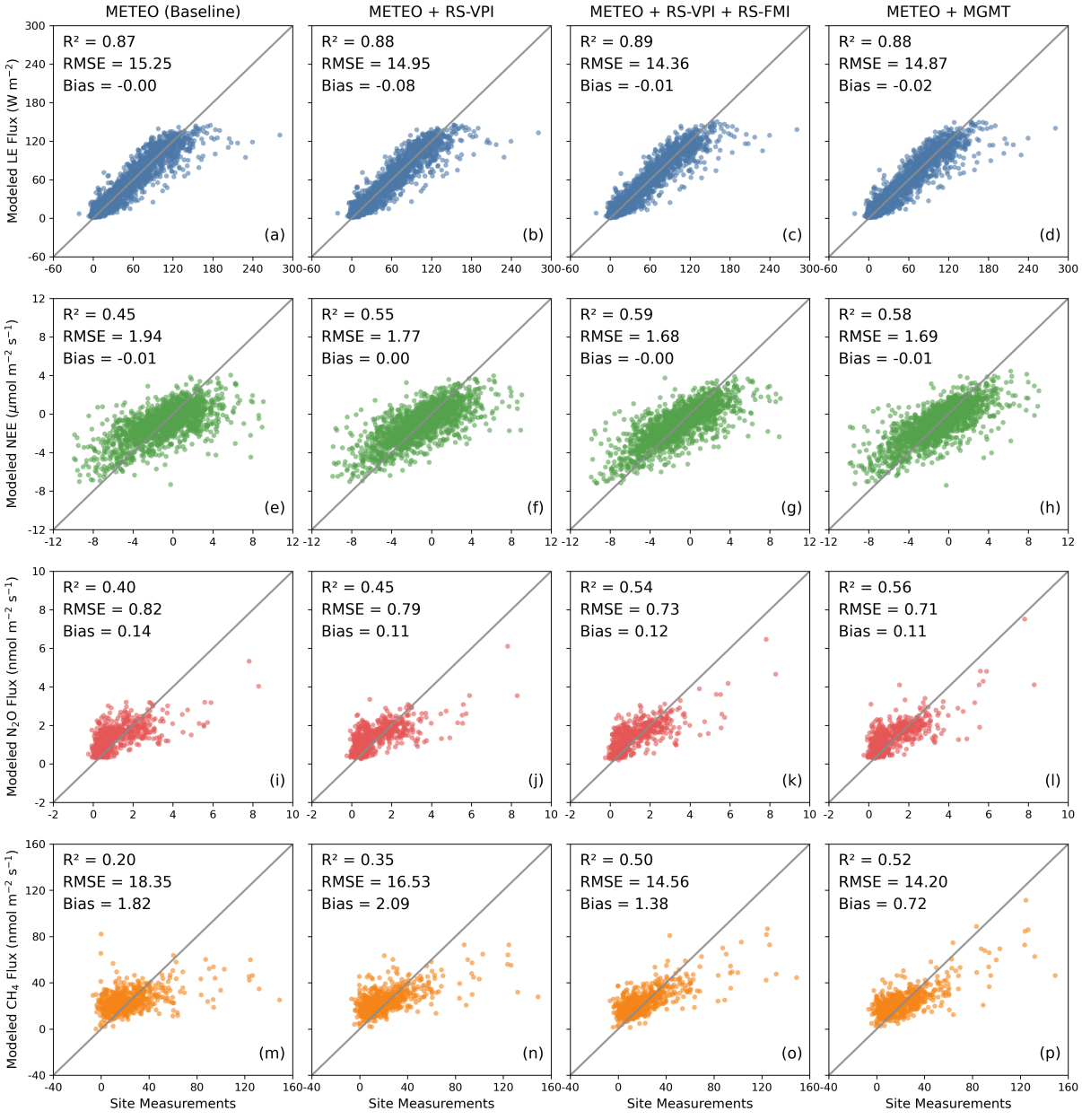


**Figure 5.** Modeled versus observed daily fluxes for four grassland sites under four scenarios. Panels show latent heat flux (LE; a–d), net ecosystem exchange of $CO_2$ (NEE; e–h), nitrous oxide flux ($N_2O$; i–l), and methane flux ($CH_4$; m–p). The four scenarios are: meteorological variables only (METEO), meteorological variables with remotely-sensed vegetation performance indicator (METEO + RS-VPI), meteorological variables with both remotely-sensed vegetation and field-management indices (METEO + RS-VPI + RS-FMIs), and meteorological variables with *in situ* management records (METEO + MGMT). Goodness of fit ($R^2$), root mean square error (RMSE) and bias are given. The grey line denotes the 1:1 relationship.

https://doi.org/10.5194/egusphere-2026-3522
Preprint. Discussion started: 26 June 2026


($R^2 = 0.59$), bringing performance close to the METEO + MGMT scenario. Scatterplots further showed compressed variability at both ends of the NEE range, with underestimation of both strong negative and high positive fluxes.

Modeling of $N_2O$ and $CH_4$ fluxes in grasslands was more challenging than for LE and NEE, with overall lower model performance in grasslands (maximum $R^2 \approx 0.56$ for $N_2O$ flux and 0.52 for $CH_4$ flux; Figure 5i–p). In the METEO-only scenario, performance was limited ($R^2 = 0.40$ for $N_2O$ and 0.20 for $CH_4$). Adding RS-VPI led to only modest improvements, whereas the inclusion of RS-FMIs resulted in substantially higher performance. For $N_2O$ flux, $R^2$ increased to 0.54 with RS-VPI + RS-FMIs, approaching the METEO + MGMT benchmark scenario ($R^2 = 0.56$). A similar pattern was observed for $CH_4$ flux, with performance improving from $R^2 = 0.20$ (METEO) to 0.50 with RS-VPI + RS-FMIs, close to the benchmark scenario ($R^2 = 0.52$). Scatterplots further showed pronounced compression at the upper range of fluxes, with systematic underestimation of high-emission events for both $N_2O$ and $CH_4$ fluxes.

Overall model performance for cropland sites was comparable to that of grasslands, with LE remaining the most accurately reproduced flux across all scenarios (Figure 6a–d). LE performance was consistently high ($R^2 = 0.86$–$0.90$), with RMSE decreasing from 15.97 W $m^{-2}$ in the METEO-only scenario to 13.26 W $m^{-2}$ when RS-VPI and RS-FMIs were included. For NEE, model performance showed clear sensitivity to the inclusion of RS-derived predictors (Figure 6e–h). The METEO-only scenario yielded moderate performance ($R^2 = 0.48$; RMSE = 2.39 $\mu$mol $CO_2$ $m^{-2}$ $s^{-1}$), while the inclusion of RS-VPI substantially improved performance ($R^2 = 0.69$; RMSE = 1.84 $\mu$mol $CO_2$ $m^{-2}$ $s^{-1}$). The addition of RS-FMIs further increased performance to $R^2 = 0.71$ with RMSE = 1.76 $\mu$mol $CO_2$ $m^{-2}$ $s^{-1}$, exceeding that of the METEO + MGMT scenario ($R^2 = 0.60$; RMSE = 2.10 $\mu$mol $CO_2$ $m^{-2}$ $s^{-1}$).

Modeling of $N_2O$ fluxes was highly scenario-dependent (Figure 6i–l). Both the METEO-only and METEO + RS-VPI scenarios showed negligible performance ($R^2 < 0.1$; RMSE > 1.05 nmol $N_2O$ $m^{-2}$ $s^{-1}$), whereas the inclusion of management information resulted in substantial improvements. The METEO + MGMT benchmark scenario achieved $R^2 = 0.57$ with RMSE = 0.71 nmol $N_2O$ $m^{-2}$ $s^{-1}$, and the METEO + RS-VPI + RS-FMIs scenario reached a comparable value ($R^2 = 0.55$; RMSE = 0.72 nmol $N_2O$ $m^{-2}$ $s^{-1}$), indicating that RS-derived management indices captured a large fraction of the explanatory information provided by site-recorded management data. For $CH_4$, performance remained modest across all scenarios ($R^2 = 0.26$–$0.37$; Figure 6m–p), with RMSE decreasing slightly from 2.92 to 2.68 nmol $CH_4$ $m^{-2}$ $s^{-1}$ when RS-derived predictors were included. The highest performance was obtained when RS-VPI and RS-FMIs were combined ($R^2 = 0.37$; RMSE = 2.68 nmol $CH_4$ $m^{-2}$ $s^{-1}$).

https://doi.org/10.5194/egusphere-2026-3522
Preprint. Discussion started: 26 June 2026


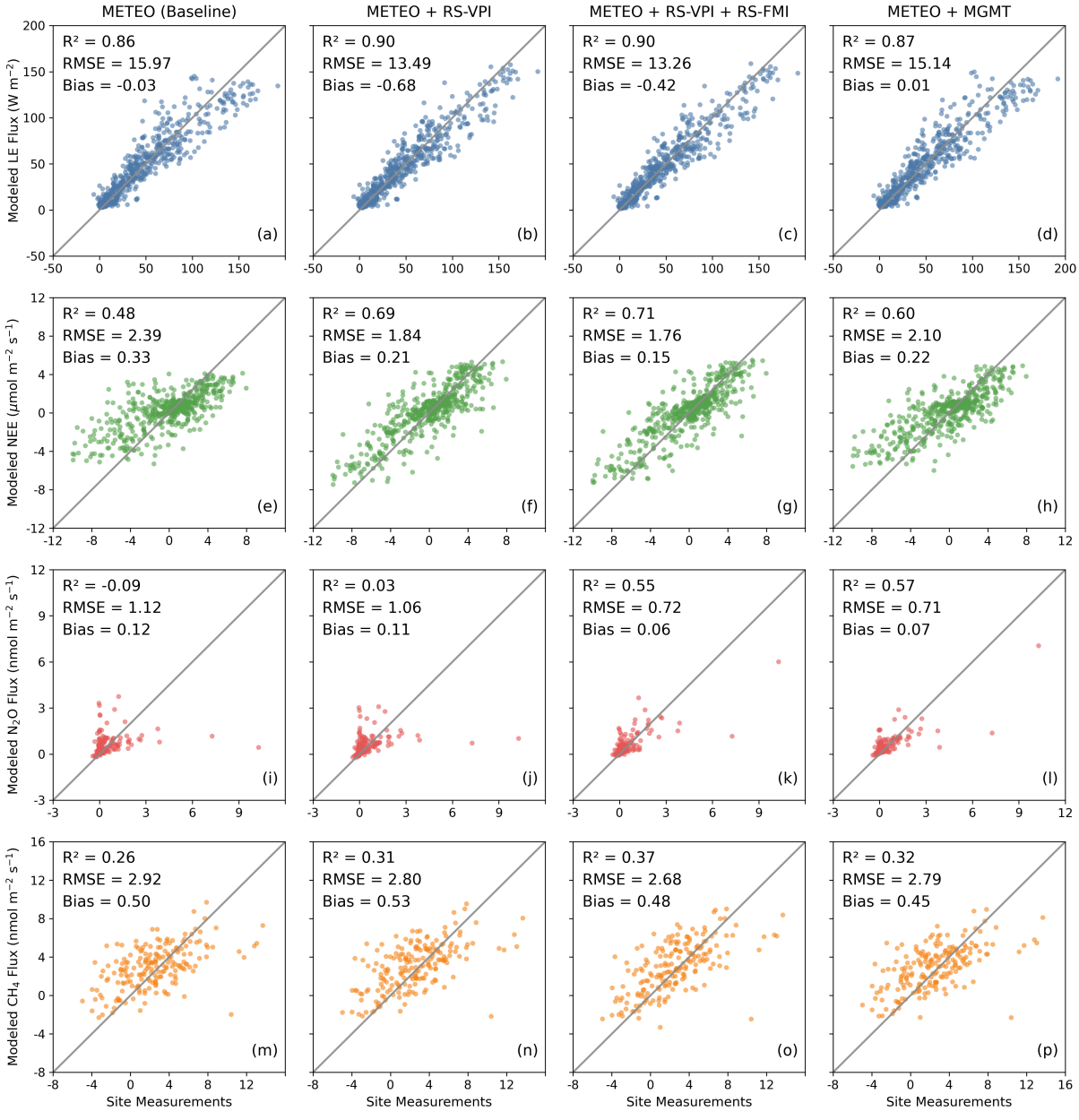


**Figure 6.** Same as Figure 5, but for the daily fluxes at two cropland sites.

Using CH-Cha and the year 2021 as an illustrative grassland example for the model with both remotely-sensed vegetation and field-management indices (METEO + RS-VPI + RS-FMIs), the time series evaluation showed that the model reproduced the seasonal trajectory and much of the intra-seasonal variability of LE and NEE, with phase agreement throughout the growing season (Figure 7). For NEE, both periods of strong $CO_2$ uptake (negative values) and net emission (positive values) were

https://doi.org/10.5194/egusphere-2026-3522
Preprint. Discussion started: 26 June 2026


reproduced in timing, although the magnitude of these extremes was underestimated. For $N_2O$ and $CH_4$ fluxes (Figure 7b–d), the model partially captures the timing of major management-related pulse events, indicating that RS-derived management indicators provide meaningful information on disturbance occurrence. However, the magnitude of these peaks is consistently underestimated, particularly for high-emission events. The pronounced $N_2O$ flux peak in August 2021 during a grassland renewal (here with vegetation destruction, shallow tillage, and reseeding) at the site is partially captured, further demonstrating that management-related disturbance signals are represented, albeit with reduced amplitude.

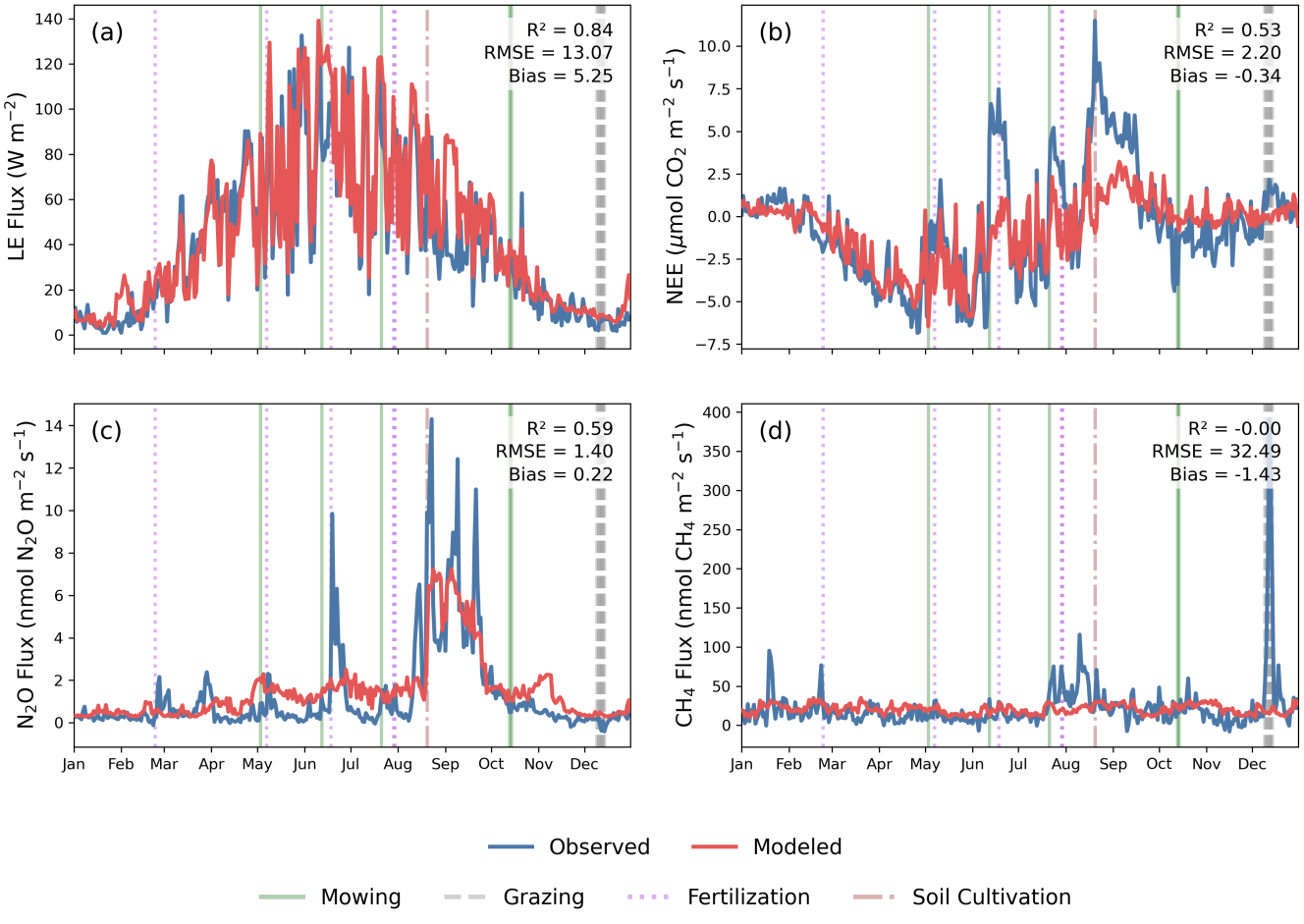


**Figure 7.** Time series at CH-Cha in 2021 comparing observed and modeled daily fluxes for (a) LE, (b) NEE, (c) $N_2O$, and (d) $CH_4$ under the METEO + RS-VPI + RS-FMIs scenario. Vertical lines indicate management events from site records (mowing, grazing, fertilization, and soil cultivation). The year 2021 with the renewal of the entire grassland in August was not included in model development as shown in Figure 5.

Overall, the time series highlighted that, while the machine learning models reproduced general temporal variability and event timing, they tended to underestimate the magnitude of extreme GHG flux responses, partly because the grassland renewal event was not represented in the model training. The comparison with non-interpolated Sentinel-2 predictors further indicated

https://doi.org/10.5194/egusphere-2026-3522
Preprint. Discussion started: 26 June 2026


a trade-off: temporal interpolation increased the number of usable daily samples and reduced clear-sky sampling bias, but it could smooth rapid management-induced vegetation changes between observations (Appendix D).

### 3.3 Driving Factor Analysis

To quantify the relative importance of different driver categories, we analyzed driver contributions using SHAP values (Figure 8) and their normalized relative contributions (Figure 9).

Across both grasslands and croplands, LE flux was consistently dominated by meteorological variables under the METEO + RS-VPI + RS-FMIs scenario (Figures 8a, b). Solar radiation had the largest SHAP values, followed by air temperature for grasslands and VPD for croplands. In contrast, vegetation- and management-related variables showed comparatively smaller contributions. This pattern was further confirmed by the grouped SHAP analysis, where meteorological drivers accounted for more than 90% of the total contribution of LE in grasslands and remained dominant in croplands (Figure 9). For NEE, the relative importance of drivers differed between agroecosystems (Figures 8c, d). In grasslands, solar radiation remained the dominant driver, whereas in croplands, LAI and bare soil period emerged as the most influential variables. The grouped SHAP results showed increased contributions from RS-derived vegetation and management indicators in croplands compared to grasslands (Figure 9), indicating a stronger role of vegetation structural dynamics.

For $N_2O$ and $CH_4$ fluxes, the SHAP patterns indicated a more complex control structure than for LE (Figures 8e–h). At the individual-variable level, both fluxes were influenced by a combination of temporally aggregated meteorological variables and RS-FMIs, such as defoliation intensity and days since defoliation. However, these effects varied between agroecosystems. For $CH_4$ fluxes, RS-FMIs and LAI played a stronger role in grasslands, whereas in croplands, the contributions remained more strongly associated with meteorological variables (Figures 8g–h). The grouped SHAP analysis further revealed how the relative explanatory contributions differed not only among fluxes but also between agroecosystems (Figure 9). While LE was consistently dominated by meteorological drivers in both systems, the contribution of RS-derived vegetation and management information increased substantially for NEE, $N_2O$, and $CH_4$ fluxes. This increase was particularly pronounced for $N_2O$ fluxes in croplands, where RS-FMIs provided the largest share of explanatory contribution. In contrast, for $CH_4$ fluxes, the contribution of RS-derived information was slightly higher in grasslands than in croplands.

https://doi.org/10.5194/egusphere-2026-3522
Preprint. Discussion started: 26 June 2026


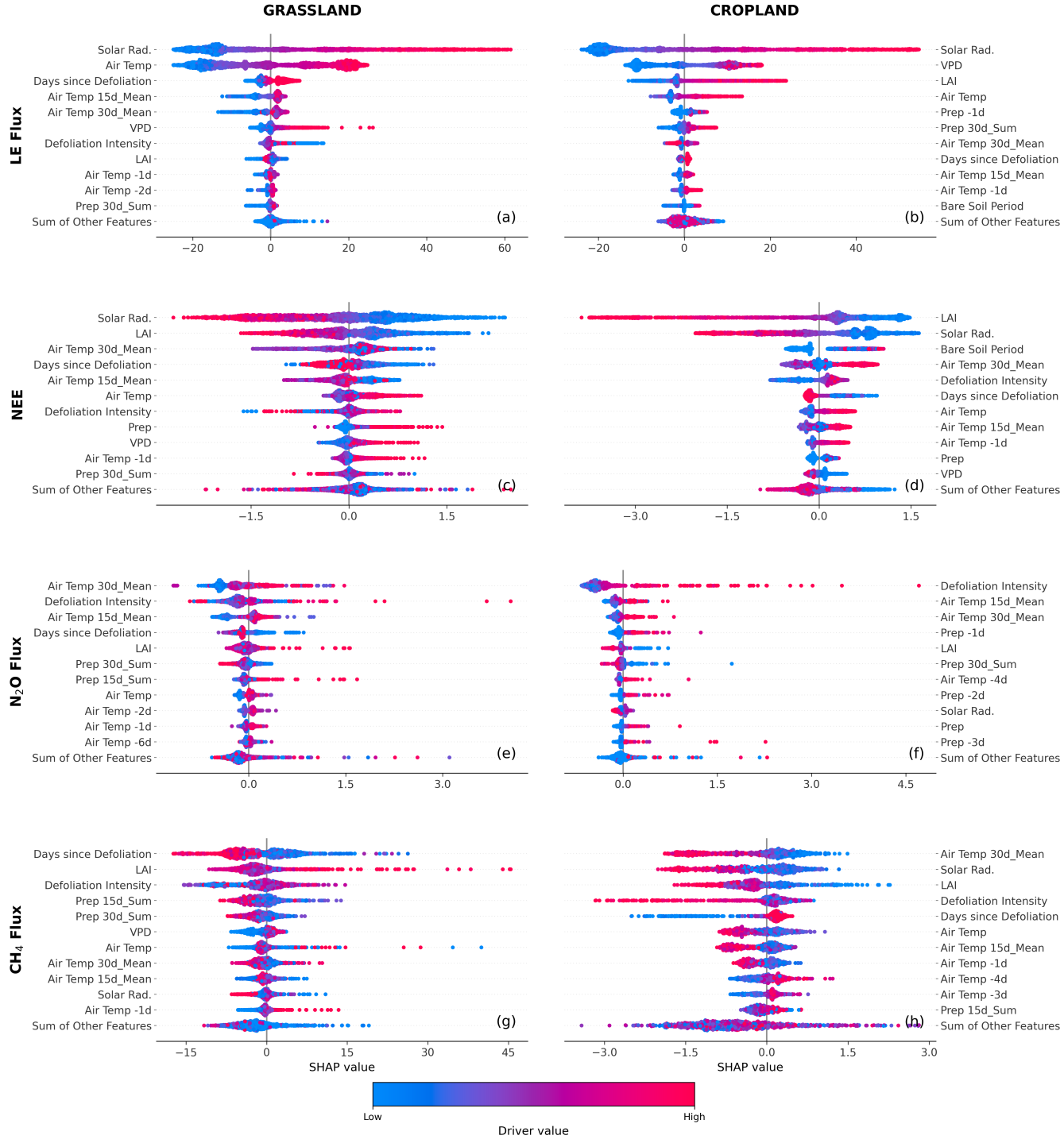


**Figure 8.** SHAP summary plots for (a, b) LE flux, (c, d) NEE, (e, f) $N_2O$ flux, and (g, h) $CH_4$ flux in grasslands (left) and croplands (right). SHAP values indicate driver contributions to model output for the METEO + RS-VPI + RS-FMIs scenario, with positive SHAP values representing positive effects on the predicted fluxes compared to the overall mean, and vice versa for negative SHAP values. Points are colored by driver value.

https://doi.org/10.5194/egusphere-2026-3522
Preprint. Discussion started: 26 June 2026


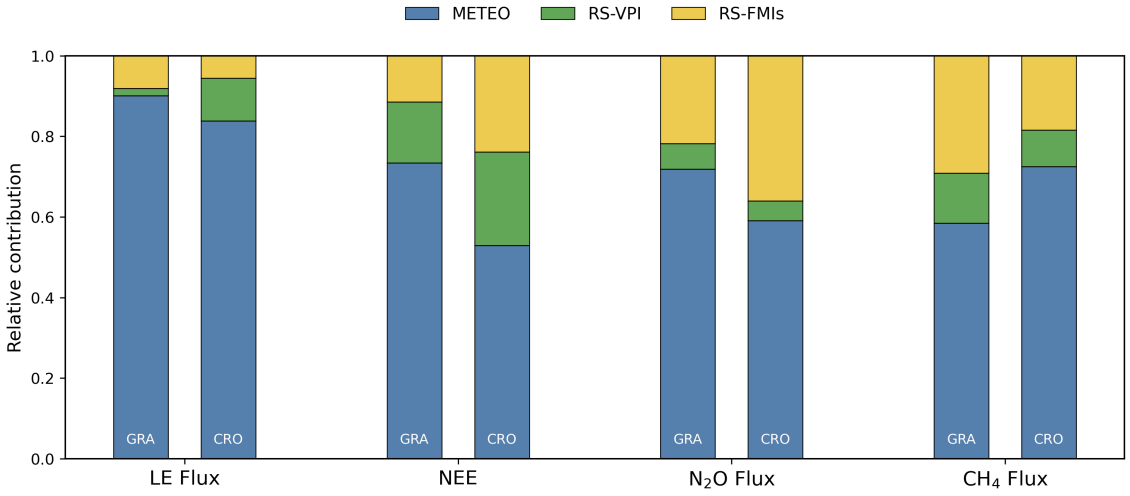


**Figure 9.** Normalized relative contributions of driver groups—meteorological variables (METEO), remotely-sensed vegetation performance index (RS-VPI), and remotely-sensed field management indices (RS-FMIs)—to LE, NEE, $N_2O$, and $CH_4$ in grasslands and croplands. Contributions are derived from absolute SHAP values aggregated by driver category for the METEO + RS-VPI + RS-FMIs scenario.

## 4 Discussion

### 4.1 Scope and Scalability of the RS-Assisted Modeling Framework

This study demonstrated that satellite-derived management and vegetation indicators can approximate part of the information contained in site management records, but its interpretation depends on several constraints related to event representation, quantitative management inputs, and environmental state variables.

LE and NEE were reproduced well ($R^2$ up to 0.90 and 0.71), addressing our third objective that RS-derived indicators add value beyond meteorology. For $N_2O$ and $CH_4$ fluxes, RS-FMIs improved performance considerably over configurations without RS information (e.g., $N_2O$ $R^2$ from below 0.1 to 0.55 in croplands), approaching the *in situ* benchmark and capturing much of the management-related variability in non-$CO_2$ fluxes (Butterbach-Bahl et al., 2013; Knox et al., 2019; Lognoul et al., 2019). The models nevertheless still underestimated high-emission events. This was consistent with the episodic nature of these fluxes, the limited representation of rare pulse events in the training data (Zhang et al., 2024), and the tendency of tree-based models to regress toward the mean (Chen and Guestrin, 2016). Similar underestimation of high-emission pulses has been reported in previous ML-based studies (Gnisia et al., 2025; Payrosangari et al., 2025; Sharma et al., 2026), reflecting a broader challenge in data-driven modeling of non-$CO_2$ fluxes. A LOSO evaluation was not implemented, because excluding an entire site would disproportionately remove specific management regimes and rare emission pulses from the training pool, making the resulting performance differences difficult to interpret.

https://doi.org/10.5194/egusphere-2026-3522
Preprint. Discussion started: 26 June 2026


The comparison with the *in situ* management benchmark showed the main advantage of RS-FMIs: they provided an approximation of management information that is available at the Swiss FluxNet sites but remains limited for regional applications (Coello et al., 2025). At the same time, both the *in situ* management metrics and RS-FMIs mainly encoded event timing and disturbance occurrence, whereas some quantitative inputs such as fertilization amount, manure composition, or livestock density were not explicitly represented in the modeling scenarios. This likely contributed to the remaining gap between correctly identifying pulse timing and reproducing pulse magnitude. The absence of high-resolution soil moisture information likely added further uncertainty, because lagged precipitation could only provide an indirect proxy for antecedent wetness rather than the soil moisture states that regulate $N_2O$ and $CH_4$ production and transport (Saha et al., 2021). Integrating RS-derived management information with process-based representations of nitrogen availability and soil biogeochemical states might help reduce this gap (Hénault et al., 2012; Sharma et al., 2026). Spatial transferability of the trained models to unobserved locations is not assessed and represents a distinct, future research objective.

### 4.2 Defoliation Intensity Index as a Proxy for Management Intensity

Previous RS-based studies have primarily focused on detecting the timing or frequency of mowing and grazing disturbances (Andreatta et al., 2022; De Vroey et al., 2022; Reinermann et al., 2020; Schwieder et al., 2022; Zhou et al., 2021). Addressing our first two objectives, the DII extended this event-based perspective by characterizing transient disturbance states from deviations between site-scale EVI dynamics and the surrounding same-land-cover vegetation background. The surrounding pixels were not assumed to be perfectly undisturbed controls; rather, they provided a local vegetation and meteorological reference against which relative defoliation disturbance and recovery could be characterized.

This background-relative formulation helped separate management-related vegetation anomalies from broader local vegetation dynamics. Unlike a binary event label, DII provided a continuous disturbance proxy that complemented Days since Defoliation by representing both the relative magnitude of canopy reduction and subsequent recovery. This made it useful for flux modeling, particularly because management effects on agroecosystem fluxes are not only controlled by event occurrence, but also by disturbance strength, recovery trajectory, and antecedent environmental conditions. Practically, DII is simple to compute, does not require a fixed event-detection threshold, and is not tied to a specific optical sensor. The normalization by local spatial variability further reduced sensitivity to absolute vegetation-performance differences across sites and seasons, improving the comparability of management-related signals within a given local context.

The event-level evaluation nevertheless indicated that DII should be interpreted as a relative spectral disturbance proxy, not as a direct estimate of harvested biomass or grazing pressure. The positive relationship between harvested biomass and DII was weaker at CH-Oe2, where crop rotation, crop-specific phenology, harvested material, and post-harvest surface conditions introduced additional spectral variability (Figure 4). In particular, grain, straw, and grass harvests are not expected to produce identical EVI responses because they differ in the fraction of photosynthetically active canopy removed and in the exposed surface conditions after harvest. Therefore, DII time series captured relative disturbance magnitude more consistently in managed grasslands, whereas cropland applications require interpretation in the context of crop identity, harvested component, and growth stage. Because recorded yields referred to management-defined harvest areas whereas DII was derived from the

https://doi.org/10.5194/egusphere-2026-3522
Preprint. Discussion started: 26 June 2026


tower-footprint-based RS sampling area, the scatterplot evaluation should be interpreted as a quantitative consistency check rather than an absolute accuracy assessment.

Several limitations follow from the formulation of DII. First, because DII is standardized by the local same-land-cover variability, its absolute magnitude should not be interpreted as a fully transferable disturbance intensity across regions with different landscape heterogeneity, crop composition, or background vegetation variability. Second, negative DII values can occur when the target field has higher EVI than the surrounding background. In this study, such negative values were mainly associated with non-harvest periods or weakly disturbed conditions, and their magnitude was generally small, often within the range of local natural variability. After restricting the event-level analysis to recorded harvest or defoliation events, negative DII values were uncommon, especially when clear, non-interpolated Sentinel-2 observations were available near the event date. These cases indicate that DII is sensitive to relative vegetation performance as well as management disturbance, and therefore event screening and observation-quality information remain important for interpretation.

The importance of RS-FMIs in the SHAP analyses (Figure 8) further suggested that management-related disturbance dynamics contributed substantially to short-term variability in non-$CO_2$ fluxes. This link is mechanistically plausible because defoliation can alter plant nitrogen uptake, labile carbon and nitrogen inputs, soil microclimate, and aeration, thereby affecting substrate availability and redox conditions relevant to $N_2O$ and $CH_4$ fluxes (Feigenwinter et al., 2023a; Maier et al., 2025). Notably, in managed agroecosystems, defoliation events are also often temporally associated with fertilization, slurry application, grazing, harvest, or soil disturbance, which can further amplify short-term emission responses. Thus, DII should be interpreted as a vegetation-derived proxy for broader disturbance states associated with management-driven biogeochemical responses, rather than as evidence that canopy reduction directly regulates $N_2O$ or $CH_4$ production.

### 4.3 Mechanistic Interpretation and Scaling Implications

The flux-dependent contribution of RS-derived information reflected distinct regulatory mechanisms across water, carbon, and non-$CO_2$ fluxes. For LE, the dominance of meteorological variables indicated that daily LE fluxes in Swiss agroecosystems operated largely within an energy-driven regime under humid temperate conditions (Jung et al., 2010; Nelson et al., 2018, 2024; Williams et al., 2012). In croplands (Figure 9), LE showed comparatively stronger sensitivity to LAI because crop emergence, canopy development, harvest, and bare soil periods produced pronounced seasonal variation in canopy structure. Such transitions strongly regulate the partitioning between soil evaporation and plant transpiration (Kelliher et al., 1995). Increasing LAI suppresses soil evaporation through shading while enhancing transpiration via increased canopy conductance, thereby altering LE partitioning even under similar atmospheric forcing (Jia et al., 2026). In contrast, grasslands maintained relatively continuous canopy cover and recovered rapidly following defoliation, resulting in weaker effective variation in canopy structure and consequently lower sensitivity of LE to LAI. Notably, irrigation is negligible in Switzerland and was therefore not considered. In arid and semi-arid regions where irrigation is a major management component, water inputs can substantially alter soil moisture, plant functioning, and associated GHG fluxes. Extending this framework to such systems would therefore require explicit representation of irrigation, for example through high-resolution LE or soil moisture products (Mwangi et al., 2026).

https://doi.org/10.5194/egusphere-2026-3522
Preprint. Discussion started: 26 June 2026


For NEE, RS-derived vegetation information reflected canopy development and vegetation transitions that regulate the balance between photosynthesis and respiration (Yin et al., 2020). In croplands, these variables tracked systematic changes in canopy structure associated with pronounced crop growth cycles, interrupted by bare soil periods after harvest and before sowing (Figure 9), which strongly constrained carbon uptake and release (Gottschalk et al., 2024). In grasslands, however, carbon exchange was less tightly linked to seasonal vegetation dynamics because canopy cover persisted throughout much of the growing season. Although canopy structure was frequently modified by management, such as mowing and grazing, it was rapidly restored, resulting in relatively small effective variation in vegetation state over time (Wang et al., 2026). As a result, vegetation information provided a stronger constraint on NEE in croplands than in grasslands.

For $N_2O$ and $CH_4$, the analyses suggested an additional layer of regulation associated with the interaction between discrete management events and antecedent environmental conditions (Figure 8). Emission peaks were frequently linked to fertilization, grazing, vegetation removal, and rainfall pulses (Feigenwinter et al., 2023a; Maier et al., 2025; Rivera and Chará, 2021; Wu et al., 2017; Zhang et al., 2021). The importance of temporally aggregated meteorological variables therefore likely reflected environmental memory rather than instantaneous forcing alone (Zhu et al., 2026). Multi-day air temperature represented antecedent thermal conditions that regulate microbial activity (Dennis et al., 2019), whereas aggregated precipitation partly reflected antecedent wetness conditions controlling gas diffusion and anaerobic microsite persistence for denitrification. Together, these results suggested that non-$CO_2$ fluxes were governed not only by meteorological variability, but by the temporal alignment between favorable environmental states and discrete management disturbances.

More broadly, this driver attribution addressed our fourth objective, showing that RS-derived vegetation and management information can provide proxies for ecosystem states and disturbance dynamics relevant to agroecosystem flux variability, thereby supporting monitoring approaches beyond sites with detailed field management records.

## 5 Conclusions

Understanding how agricultural management interacts with meteorological forcing to regulate water and greenhouse gas fluxes remains a central challenge in ecosystem modeling, particularly because incomplete management records limit accurate budget estimation. This study showed that the value of integrating remotely-sensed vegetation and management indicators was fundamentally flux-dependent, revealing a clear hierarchy of controls across Swiss grassland and cropland systems. While daily evapotranspiration was primarily constrained by atmospheric demand and energy availability, carbon dioxide, nitrous oxide, and methane fluxes were additionally shaped by antecedent meteorological conditions, vegetation state, and the timing and intensity of management events. By explicitly incorporating satellite-derived vegetation dynamics and disturbance signals, the proposed framework disentangled the relative roles of climate forcing and management-driven ecosystem states in regulating flux variability. Beyond improving predictive performance, these results highlight the broader potential of remote-sensing-informed management representations for monitoring agricultural greenhouse gas fluxes. Satellite observations provide a pathway for regional monitoring of agroecosystem fluxes and the reconstruction of historical management regimes. Future advances integrating high-resolution remote sensing with hybrid process–data approaches, improved soil moisture constraints,

https://doi.org/10.5194/egusphere-2026-3522
Preprint. Discussion started: 26 June 2026


and multi-sensor observations will further strengthen the attribution of management effects on ecosystem fluxes. Such advances are critical for building next-generation monitoring frameworks capable of supporting climate mitigation strategies, sustainable agricultural management, and transparent reporting of agricultural emissions under accelerating environmental change.

*Code and data availability.* *In situ* measurements are available from the ICOS Data Portal and the ETH Research Collection. Sentinel-2 Level-2 surface reflectance products are publicly available from the Copernicus Data Space Ecosystem. The Sentinel-2–based mowing detection algorithm used in this study is implemented within the FORCE framework and is available at https://github.com/davidfrantz/force-udf/tree/main/python/ts/mowingDetection (last access: 15 June 2026). The *in situ* flux data processing is documented in a representative pipeline at https://holukas.github.io/dataset_ch-cha_flux_product/intro.html (last access: 15 June 2026). The additional analysis scripts developed for this study are available from the corresponding author upon reasonable request.

## Appendix A: Evaluation of Remotely-Sensed Defoliation Event Detection

The EVI-based defoliation detection method showed low commission error, with most detected events matching recorded mowing activities (Figure A1a). However, the algorithm appeared relatively conservative and failed to detect some mowing or grazing events. Therefore, the development of an index to quantify mowing intensity remains necessary. Moreover, due to the lack of Sentinel-2 observations during prolonged cloudy periods in winter, multi-day winter grazing events are typically missed.

https://doi.org/10.5194/egusphere-2026-3522
Preprint. Discussion started: 26 June 2026


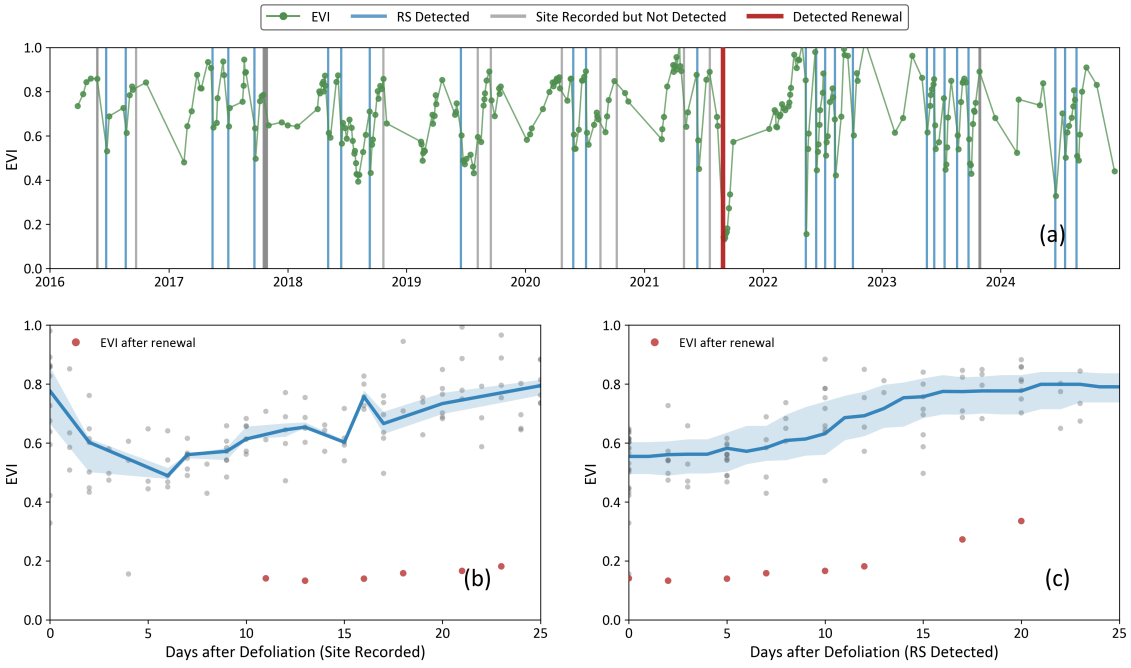


**Figure A1.** Evaluation of the RS-based defoliation detection at the CH-Cha site. (a) EVI time series from 2016 to 2024, with RS-detected defoliation events matched to site records shown in blue, site-recorded defoliation events not detected by RS shown in grey, and the detected renewal event highlighted in red; site-recorded events without valid EVI observations within ±10 days were not annotated. (b) EVI recovery following site-recorded defoliation events. (c) EVI recovery following RS-detected events. In (b) and (c), grey points show individual EVI observations, the solid blue line shows the daily median, and the shaded area shows the interquartile range; a ±3-day temporal mismatch tolerance was allowed when comparing RS-detected and site-recorded events. Red points indicate EVI observations after the August 2021 renewal event.

The EVI recovery following site-recorded mowing or grazing showed a clear swoosh-shaped pattern (Figure A1b). EVI continued to decline during the first few days after the recorded management event, likely because harvested grass was often left on the ground to dry before removal, producing a delayed minimum in the vegetation signal. A consistent recovery phase started after approximately 3–5 days. The recovery trajectory based on RS-detected events showed a similar overall pattern, but was shifted slightly later by about 3 days (Figure A1c). This shift was expected because the RS detection relied on a sufficiently strong post-defoliation spectral signal, which may become most apparent only after the cut biomass had dried or after the next valid satellite observation. The red recovery trace in Figure A1b–c corresponds to the August 2021 renewal event, which was a significant defoliation event; thus, the related EVI values are scattered.

https://doi.org/10.5194/egusphere-2026-3522
Preprint. Discussion started: 26 June 2026


## Appendix B: Sensitivity of DII to Spatial Window Size

Because the Defoliation Intensity Index (DII) is derived from spatial aggregation of EVI within a defined neighborhood, its behavior depends on the selected spatial window size. A window that is too small may not adequately represent the local background vegetation state, whereas an overly large window may reduce comparability with site-level conditions and introduce confounding effects from terrain heterogeneity, mixed land cover, or management regimes unrelated to the flux footprint. To evaluate the sensitivity of DII to spatial window size, we varied the diameter of the spatial window from 200 m to 5000 m (Figure B1). For each diameter, DII was recalculated and incorporated into the modeling framework, and predictive performance was assessed using $R^2$ for each flux type across grassland and cropland systems.

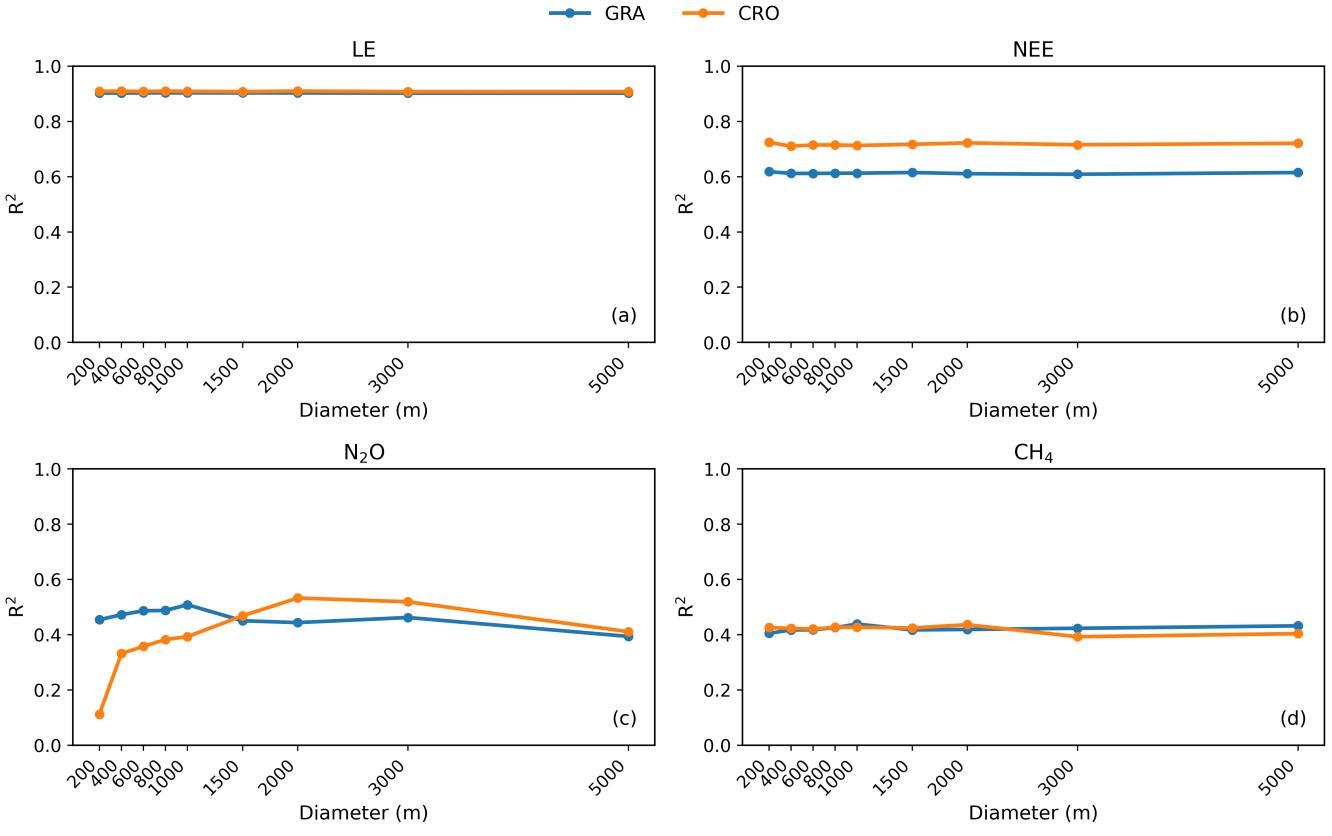


**Figure B1.** Sensitivity of model performance ($R^2$) to the spatial window diameter used in the Defoliation Intensity Index (DII) calculation for grassland (GRA) and cropland (CRO) systems.

The sensitivity analysis showed that the influence of spatial window size varied across flux variables and ecosystem types. LE, NEE, and $CH_4$ showed limited sensitivity to the selected window size, whereas $N_2O$ showed the strongest response. For LE, model performance remained nearly constant across all tested diameters, reflecting the dominant role of meteorological

https://doi.org/10.5194/egusphere-2026-3522
Preprint. Discussion started: 26 June 2026


forcing in controlling latent heat flux. NEE and $CH_4$ also showed relatively stable $R^2$ values once the window diameter exceeded several hundred meters, indicating that the vegetation and management signals captured within these spatial scales were sufficient to represent much of their variability.

In contrast, $N_2O$ flux exhibited stronger sensitivity to the spatial window size. Model performance increased with increasing diameter up to a certain scale, beyond which it stabilized or slightly declined. The optimal spatial scale differed between ecosystem types: for grasslands, model performance was highest and most stable at approximately 1 km diameter, whereas for croplands the optimum shifted toward approximately 2 km. This difference likely reflected contrasting landscape structure and management scales between the two systems. Grassland sites are often embedded in more heterogeneous terrain, where smaller windows better preserve local representativeness. Cropland sites are generally located in flatter lowland landscapes with larger management units, where broader windows better capture the relevant background vegetation state.

Based on this analysis, a 1 km diameter was adopted for grassland sites and a 2 km diameter for cropland sites. This window-size selection should be interpreted as site-specific to the Swiss FluxNet sites used here; the optimal spatial scale may differ in other regions with different field sizes, terrain conditions, crop types, and management regimes.

## Appendix C: Selected XGBoost parameter schemes

Final XGBoost parameter schemes were selected separately for each target variable and for grassland and cropland models (Table C1). Parameter selection was conducted independently. Although tuning was initially conducted for each scenario, the selected parameter sets were similar across scenarios; therefore, for final reporting, we adopted one parameter scheme per target variable and ecosystem type to avoid introducing additional variability and to enable a straightforward comparison of model performance. The optimal scheme was identified based on repeated site-stratified cross-validation (10-fold, 5 repeats), using $R^2$ summarized by the criterion of mean minus half standard deviation.

**Table C1.** Selected XGBoost parameter schemes for grassland and cropland models.

| | Grassland | | | | Cropland | | | |
|---|---|---|---|---|---|---|---|---|
| Parameter | LE | NEE | $N_2O$ | $CH_4$ | LE | NEE | $N_2O$ | $CH_4$ |
| n_estimators | 200 | 200 | 400 | 400 | 200 | 400 | 400 | 400 |
| learning_rate | 0.03 | 0.03 | 0.02 | 0.02 | 0.03 | 0.02 | 0.02 | 0.02 |
| max_depth | 3 | 3 | 7 | 7 | 4 | 8 | 8 | 8 |
| min_child_weight | 10 | 10 | 4 | 4 | 6 | 3 | 3 | 3 |
| subsample | 0.55 | 0.55 | 0.75 | 0.75 | 0.65 | 0.80 | 0.80 | 0.80 |
| colsample | 0.55 | 0.55 | 0.75 | 0.75 | 0.65 | 0.80 | 0.80 | 0.80 |
| gamma | 10 | 10 | 2 | 2 | 5 | 1 | 1 | 1 |
| $\lambda$ | 20.0 | 20.0 | 5.0 | 5.0 | 10.0 | 3.0 | 3.0 | 3.0 |
| $\alpha$ | 8.0 | 8.0 | 1.0 | 1.0 | 4.0 | 0.5 | 0.5 | 0.5 |

https://doi.org/10.5194/egusphere-2026-3522
Preprint. Discussion started: 26 June 2026


The selected hyperparameter regimes showed broadly consistent grouping across flux types. LE and NEE generally favored relatively constrained configurations, whereas $N_2O$ and $CH_4$ fluxes required more flexible regimes with deeper trees, weaker regularization, and longer boosting. For LE and NEE, the optimal configuration was characterized by shallow trees (max depth = 3), strong regularization (high $\gamma$, $\lambda$, and $\alpha$), and moderate boosting length. This combination indicated that model performance was maximized under a constrained representation, suggesting that the dominant relationships can be captured by relatively smooth and low-complexity functions.

In contrast, for both $N_2O$ and $CH_4$ fluxes, a more flexible configuration was selected, including deeper trees (max depth = 7), reduced regularization, and longer boosting with a smaller learning rate. This regime allowed the model to capture stronger nonlinearity and interaction effects, which are required to reproduce the variability in these fluxes. Lower values of `min_child_weight` in the $N_2O$ and $CH_4$ models allowed splits based on smaller subsets of samples, which facilitated the representation of rare but high-magnitude events. In contrast, higher values selected for LE and NEE enforced splits supported by larger sample sizes, leading to smoother predictions and improved generalization.

The contrast in selected hyperparameter regimes between LE/NEE and $N_2O$/$CH_4$ was consistent with differences in their statistical characteristics. LE and NEE typically exhibited smoother temporal dynamics and comparatively stable distributions, which could be effectively captured using strongly regularized, low-complexity models. In contrast, $N_2O$ and $CH_4$ fluxes were characterized by higher variability, pronounced skewness, and intermittent high-magnitude events. Capturing such behavior required more flexible model configurations, including deeper trees, reduced regularization, and longer boosting, allowing the model to represent nonlinear interactions and extreme responses.

## Appendix D: Evaluation of Sentinel-2 Temporal Interpolation

Temporal discontinuity of RS drivers introduces two related limitations. First, optical RS acquisitions are irregular and preferentially occur under clear-sky conditions, which can over-represent high-radiation periods and under-sample cloudy or transitional conditions (Jia et al., 2024). Because incoming radiation strongly controls both LE and NEE, this sampling structure can bias the representation of continuous flux dynamics. Second, the temporal gaps between acquisitions limit the ability to resolve rapid vegetation and management-induced changes. To obtain daily coverage and reduce this sampling bias, RS products were temporally interpolated. Although this step enabled continuous flux modeling, its influence on model performance and uncertainty required further evaluation.

The sensitivity analysis illustrated why interpolation cannot simply be omitted (Figure D1). Under the same training and evaluation protocol, the model retained some seasonal correspondence at available RS acquisition dates, but predictive skill deteriorated and large temporal gaps remained at CH-Cha. However, restricting the analysis to actual RS acquisition dates reduced the number of valid prediction days and left large temporal gaps. Thus, omitting interpolation replaced interpolation-related smoothing with sparse and biased sampling, rather than removing uncertainty. Improved high-resolution RS time-series reconstruction, including multi-sensor fusion and advanced gap-filling approaches (e.g., temperature response curve–based

https://doi.org/10.5194/egusphere-2026-3522
Preprint. Discussion started: 26 June 2026


reconstruction (Tschurr et al., 2025)), will therefore be needed to better capture short-lived flux responses associated with management disturbances.

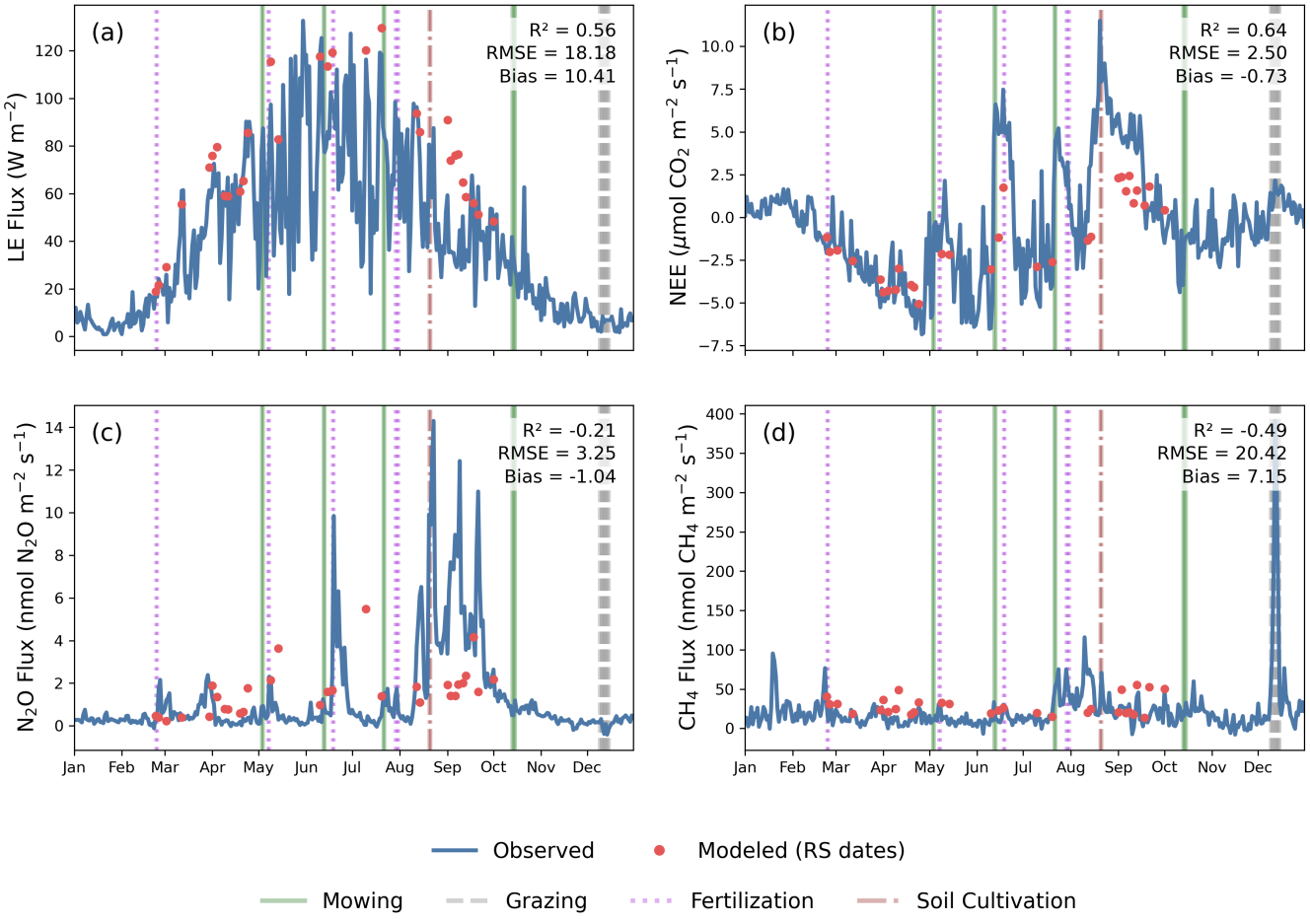


**Figure D1.** Same as Figure 7, but using non-interpolated RS records for model training and prediction.

*Author contributions.* A.J.: Conceptualization, Methodology, Software, Formal analysis, Data curation, Validation, Visualization, Writing – original draft. H.A.: Conceptualization, Supervision, Funding acquisition, Methodology. L.H., I.F., K.-M.K., F. Tschurr, L.A., F. Turco: Data curation, Investigation. S.L., T.L.: Data curation, Software. N.B.: Conceptualization, Supervision, Funding acquisition. All authors: Writing – review & editing.

*Competing interests.* The authors declare that they have no competing interests.

https://doi.org/10.5194/egusphere-2026-3522
Preprint. Discussion started: 26 June 2026


*Acknowledgements.* This study was financed by the PERSIST project (Spatio-Temporal Patterns and Trends of Environmental Footprints and Reductions of Climate Impacts in Switzerland) within the Smart Farming Research Program of the World Food System Center, supported by fenaco and the ETH Zürich Foundation (Grant No. 2025-HS-232) awarded to N.B. and H.A.. This work was made possible by using the Swiss Agricultural Landscape Intelligence Platform established and maintained by Agroscope. I.F. acknowledges funding from the Swiss National Science Foundation (20FI0_229655, project ICOS-CH Phase 4). T.L. was financed by the Crop1990 project awarded to H.A. by the Federal Office for the Environment (FOEN) (06.0091.PZ/0046). We gratefully acknowledge the technical support provided for the maintenance of the eddy-covariance stations by Peter Ravelhofer, Thomas Baur, Philip Meier, Martin Rüegg, and Eric Brouwer. We thank Drs. Jake Nelson, Sophia Walther, José Grünzweig, Marius G. Floriancic, and Yu Zhou for valuable discussion. The authors used generative AI tools to assist with language editing. All scientific content and conclusions were verified by the authors.

https://doi.org/10.5194/egusphere-2026-3522
Preprint. Discussion started: 26 June 2026


## References

Aasen, H., Honkavaara, E., Lucieer, A., and Zarco-Tejada, P. J.: Quantitative remote sensing at ultra-high resolution with UAV spectroscopy: a review of sensor technology, measurement procedures, and data correction workflows, Remote Sensing, 10, 1091, 2018.

Andreatta, D., Gianelle, D., Scotton, M., Vescovo, L., and Dalponte, M.: Detection of grassland mowing frequency using time series of vegetation indices from Sentinel-2 imagery, GIScience & Remote Sensing, 59, 481–500, 2022.

Atzberger, C., Darvishzadeh, R., Immitzer, M., Schlerf, M., Skidmore, A., and Le Maire, G.: Comparative analysis of different retrieval methods for mapping grassland leaf area index using airborne imaging spectroscopy, International Journal of Applied Earth Observation and Geoinformation, 43, 19–31, 2015.

Baldocchi, D., Falge, E., Gu, L., Olson, R., Hollinger, D., Running, S., Anthoni, P., Bernhofer, C., Davis, K., and Evans, R.: FLUXNET: a new tool to study the temporal and spatial variability of ecosystem-scale carbon dioxide, water vapor, and energy flux densities, Bulletin of the American Meteorological Society, 82, 2415–2434, 2001.

Baldocchi, D. D., Hincks, B. B., and Meyers, T. P.: Measuring biosphere-atmosphere exchanges of biologically related gases with micrometeorological methods, Ecology, 69, 1331–1340, 1988.

Buchmann, N., Fuchs, K., Feigenwinter, I., and Gilgen, A. K.: Multifunctionality of permanent grasslands: ecosystem services and resilience to climate change, Grassland Science in Europe, 24, 19–26, 2019.

Buchmann, N., Hörtnagl, L., Zeeman, M., Fuchs, K., Feigenwinter, I., Burri, S., Baur, T., and Meier, P.: Fluxnet archive product from Fruebuel, 2005–2024, https://hdl.handle.net/11676/xnRKIWdx6isC5GLqv_pHq5hU, 2025.

Buchmann, N., Hörtnagl, L., Kohonen, K.-M., Zeeman, M., Ghiasi, S., Baur, T., and Meier, P.: Fluxnet archive product from Alp Weissenstein, 2006–2024, https://hdl.handle.net/11676/2c8FDF30wAcPfPTgr_PwL3qv, 2026a.

Buchmann, N., Hörtnagl, L., Maier, R., Turco, F., Baur, T., and Meier, P.: Fluxnet archive product from Oensingen crop, 2004–2024, https://hdl.handle.net/11676/nayPPdWP7UC3vBVNv1HnbxOJ, 2026b.

Bundesamt für Landwirtschaft (BLW): Landwirtschaftliche Kulturflächen, https://www.blw.admin.ch/de/landwirtschaftliche-kulturflaechen, 2024.

Butterbach-Bahl, K., Baggs, E. M., Dannenmann, M., Kiese, R., and Zechmeister-Boltenstern, S.: Nitrous oxide emissions from soils: how well do we understand the processes and their controls?, Philosophical Transactions of the Royal Society B: Biological Sciences, 368, 2013.

Chen, J. M. and Liu, J.: Evolution of evapotranspiration models using thermal and shortwave remote sensing data, Remote Sensing of Environment, 237, 111 594, 2020.

Chen, T. and Guestrin, C.: XGBoost: a scalable tree boosting system, in: Proceedings of the 22nd ACM SIGKDD international conference on knowledge discovery and data mining, pp. 785–794, 2016.

Coello, F., Decorte, T., Janssens, I., Mortier, S., Sardans, J., Peñuelas, J., and Verdonck, T.: Global crop-specific fertilization dataset from 1961–2019, Scientific Data, 12, 40, 2025.

De Vroey, M., de Vendictis, L., Zavagli, M., Bontemps, S., Heymans, D., Radoux, J., Koetz, B., and Defourny, P.: Mowing detection using Sentinel-1 and Sentinel-2 time series for large scale grassland monitoring, Remote Sensing of Environment, 280, 113 145, 2022.

Dennis, P. G., Newsham, K. K., Rushton, S. P., O'Donnell, A. G., and Hopkins, D. W.: Soil bacterial diversity is positively associated with air temperature in the maritime Antarctic, Scientific Reports, 9, 2686, 2019.

https://doi.org/10.5194/egusphere-2026-3522
Preprint. Discussion started: 26 June 2026


Dietiker, D., Buchmann, N., and Eugster, W.: Testing the ability of the DNDC model to predict $CO_2$ and water vapour fluxes of a Swiss cropland site, Agriculture, Ecosystems & Environment, 139, 396–401, 2010.

Dusseux, P., Vertès, F., Corpetti, T., Corgne, S., and Hubert-Moy, L.: Agricultural practices in grasslands detected by spatial remote sensing, Environmental Monitoring and Assessment, 186, 8249–8265, 2014.

Emmel, C., Winkler, A., Hörtnagl, L., Revill, A., Ammann, C., D'Odorico, P., Buchmann, N., and Eugster, W.: Integrated management of a Swiss cropland is not sufficient to preserve its soil carbon pool in the long term, Biogeosciences, 15, 5377–5393, 2018.

Eugster, W. and Merbold, L.: Eddy covariance for quantifying trace gas fluxes from soils, Soil, 1, 187–205, 2015.

Feigenwinter, I., Hörtnagl, L., and Buchmann, N.: $N_2O$ and $CH_4$ fluxes from intensively managed grassland: The importance of biological and environmental drivers vs. management, Science of the Total Environment, 903, 166 389, 2023a.

Feigenwinter, I., Hörtnagl, L., Zeeman, M. J., Eugster, W., Fuchs, K., Merbold, L., and Buchmann, N.: Large inter-annual variation in carbon sink strength of a permanent grassland over 16 years: Impacts of management practices and climate, Agricultural and Forest Meteorology, 340, 109 613, 2023b.

Gaillard, R. K., Jones, C. D., Ingraham, P., Collier, S., Izaurralde, R. C., Jokela, W., Osterholz, W., Salas, W., Vadas, P., and Ruark, M. D.: Underestimation of $N_2O$ emissions in a comparison of the DayCent, DNDC, and EPIC models, Ecological Applications, 28, 694–708, 2018.

Gnisia, G., Weik, J., Ruser, R., Essich, L., Lewandowski, I., and Stein, A.: Machine learning-based prediction of nitrous oxide emissions from arable farming: Exploring management practices as predictor variables, Ecological Indicators, 172, 113 233, 2025.

Gottschalk, P., Kalhori, A., Li, Z., Wille, C., and Sachs, T.: Monitoring cropland daily carbon dioxide exchange at field scales with Sentinel-2 satellite imagery, Biogeosciences, 21, 3593–3616, 2024.

Graf, L. V., Merz, Q. N., Walter, A., and Aasen, H.: Insights from field phenotyping improve satellite remote sensing based in-season estimation of winter wheat growth and phenology, Remote Sensing of Environment, 299, 113 860, 2023.

Guo, Y., Zhang, G., Abdalla, M., Kuhnert, M., Bao, H., Xu, H., Ma, J., Begum, K., and Smith, P.: Modelling methane emissions and grain yields for a double-rice system in Southern China with DAYCENT and DNDC models, Geoderma, 431, 116 364, 2023.

Hastings, A. F., Wattenbach, M., Eugster, W., Li, C., Buchmann, N., and Smith, P.: Uncertainty propagation in soil greenhouse gas emission models: an experiment using the DNDC model and at the Oensingen cropland site, Agriculture, Ecosystems & Environment, 136, 97–110, 2010.

Heimsch, L., Vira, J., Fer, I., Vekuri, H., Tuovinen, J.-P., Lohila, A., Liski, J., and Kulmala, L.: Impact of weather and management practices on greenhouse gas flux dynamics on an agricultural grassland in Southern Finland, Agriculture, Ecosystems & Environment, 374, 109 179, 2024.

Heiskanen, J., Brümmer, C., Buchmann, N., Calfapietra, C., Chen, H., Gielen, B., Gkritzalis, T., Hammer, S., Hartman, S., and Herbst, M.: The integrated carbon observation system in Europe, Bulletin of the American Meteorological Society, 103, E855–E872, 2022.

Hénault, C., Grossel, A., Mary, B., Roussel, M., and Léonard, J.: Nitrous oxide emission by agricultural soils: a review of spatial and temporal variability for mitigation, Pedosphere, 22, 426–433, 2012.

Henne, S., Brunner, D., Oney, B., Leuenberger, M., Eugster, W., Bamberger, I., Meinhardt, F., Steinbacher, M., and Emmenegger, L.: Validation of the Swiss methane emission inventory by atmospheric observations and inverse modelling, Atmospheric Chemistry and Physics, 16, 3683–3710, 2016.

Hörtnagl, L., Barthel, M., Buchmann, N., Eugster, W., Butterbach-Bahl, K., Díaz-Pinés, E., Zeeman, M., Klumpp, K., Kiese, R., and Bahn, M.: Greenhouse gas fluxes over managed grasslands in Central Europe, Global Change Biology, 24, 1843–1872, 2018.

https://doi.org/10.5194/egusphere-2026-3522
Preprint. Discussion started: 26 June 2026


Hörtnagl, L., Feigenwinter, I., Wang, Y., Buchmann, N., Merbold, L., Zeeman, M., Fuchs, K., and Eugster, W.: Eddy covariance ecosystem fluxes, meteorological data and detailed management information for the intensively managed grassland site Chamau in Switzerland, collected between 2005 and 2024, https://doi.org/10.3929/ETHZ-B-000747025, 2025.

Ivanova, K., Virkkala, A.-M., Brovkin, V., Stacke, T., Widhalm, B., Bartsch, A., Voigt, C., Sonnentag, O., and Göckede, M.: High-resolution remote sensing and machine-learning-based upscaling of methane fluxes: a case study in the Western Canadian tundra, Biogeosciences, 23, 233–262, 2026.

Jacquemoud, S., Verhoef, W., Baret, F., Bacour, C., Zarco-Tejada, P. J., Asner, G. P., François, C., and Ustin, S. L.: PROSPECT + SAIL models: a review of use for vegetation characterization, Remote Sensing of Environment, 113, S56–S66, 2009.

Jia, A., Liang, S., Wang, D., Mallick, K., Zhou, S., Hu, T., and Xu, S.: Advances in methodology and generation of all-weather land surface temperature products from polar-orbiting and geostationary satellites: a comprehensive review, IEEE Geoscience and Remote Sensing Magazine, 12, 218–260, https://doi.org/10.1109/MGRS.2024.3421268, 2024.

Jia, A., Mallick, K., Upadhyaya, D., Hu, T., Szantoi, Z., Bhattacharya, B., Sekhar, M., Skoković, D., Sobrino, J. A., Ruiz, L., and Boulet, G.: Deriving a clear-sky soil moisture index from ECOSTRESS land surface temperature, Remote Sensing of Environment, 329, 114 945, https://doi.org/10.1016/j.rse.2025.114945, 2025.

Jia, A., Mallick, K., Lin, Z., Sulis, M., Szantoi, Z., Zhang, L., Corbari, C., Munoz, P. T., Nieto, H., Roujean, J.-L., Etchanchu, J., Demarty, J., Mwangi, S., Olioso, A., Merlin, O., and Boulet, G.: Sensitivity of thermal evapotranspiration models to surface and atmospheric drivers across ecosystems and aridity, Agricultural and Forest Meteorology, 376, 110 930, 2026.

Jung, M., Reichstein, M., Ciais, P., Seneviratne, S. I., Sheffield, J., Goulden, M. L., Bonan, G., Cescatti, A., Chen, J., and De Jeu, R.: Recent decline in the global land evapotranspiration trend due to limited moisture supply, Nature, 467, 951–954, 2010.

Jung, M., Schwalm, C., Migliavacca, M., Walther, S., Camps-Valls, G., Koirala, S., Anthoni, P., Besnard, S., Bodesheim, P., and Carvalhais, N.: Scaling carbon fluxes from eddy covariance sites to globe: synthesis and evaluation of the FLUXCOM approach, Biogeosciences, 17, 1343–1365, 2020.

Karlshoefer, P., d'Angelo, P., Eberle, J., and Heiden, U.: Evaluation framework for the generation of continental bare surface reflectance composites, Geoderma, 459, 117 340, 2025.

Kelliher, F. M., Leuning, R., Raupach, M., and Schulze, E.-D.: Maximum conductances for evaporation from global vegetation types, Agricultural and Forest Meteorology, 73, 1–16, 1995.

Kljun, N., Calanca, P., Rotach, M. W., and Schmid, H. P.: A simple two-dimensional parameterisation for Flux Footprint Prediction (FFP), Geoscientific Model Development, 8, 3695–3713, 2015.

Knox, S. H., Jackson, R. B., Poulter, B., McNicol, G., Fluet-Chouinard, E., Zhang, Z., Hugelius, G., Bousquet, P., Canadell, J. G., Saunois, M., et al.: FLUXNET-$CH_4$ synthesis activity: objectives, observations, and future directions, Bulletin of the American Meteorological Society, 100, 2607–2632, 2019.

Law, B. E., Falge, E., Gu, L., Baldocchi, D. D., Bakwin, P., Berbigier, P., Davis, K., Dolman, A. J., Falk, M., and Fuentes, J. D.: Environmental controls over carbon dioxide and water vapor exchange of terrestrial vegetation, Agricultural and Forest Meteorology, 113, 97–120, 2002.

Liang, S., He, T., Huang, J., Jia, A., Zhang, Y., Cao, Y., Chen, X., Chen, X., Cheng, J., and Jiang, B.: Advances in high-resolution land surface satellite products: a comprehensive review of inversion algorithms, products and challenges, Science of Remote Sensing, p. 100152, 2024.

Lobert, F., Schwieder, M., Alsleben, J., Broeg, T., Kowalski, K., Okujeni, A., Hostert, P., and Erasmi, S.: Unveiling year-round cropland cover by soil-specific spectral unmixing of Landsat and Sentinel-2 time series, Remote Sensing of Environment, 318, 114 594, 2025.

https://doi.org/10.5194/egusphere-2026-3522
Preprint. Discussion started: 26 June 2026


Lognoul, M., Debacq, A., De Ligne, A., Dumont, B., Manise, T., Bodson, B., Heinesch, B., and Aubinet, M.: $N_2O$ flux short-term response to temperature and topsoil disturbance in a fertilized crop: an eddy covariance campaign, Agricultural and Forest Meteorology, 271, 193–206, 2019.

Lundberg, S. M. and Lee, S.-I.: A unified approach to interpreting model predictions, Advances in Neural Information Processing Systems, 30, 2017.

Maier, R., Hörtnagl, L., and Buchmann, N.: Greenhouse gas fluxes ($CO_2$, $N_2O$ and $CH_4$) of pea and maize during two cropping seasons: drivers, budgets, and emission factors for nitrous oxide, Science of the Total Environment, 849, 157 541, 2022.

Maier, R., Hörtnagl, L., and Buchmann, N.: Large nitrous oxide emissions from arable soils after crop harvests prior to sowing, Nutrient Cycling in Agroecosystems, 130, 161–175, 2025.

Mathers, C., Black, C. K., Segal, B. D., Gurung, R. B., Zhang, Y., Easter, M. J., Williams, S., Motew, M., Campbell, E. E., and Brummitt, C. D.: Validating DayCent-CR for cropland soil carbon offset reporting at a national scale, Geoderma, 438, 116 647, 2023.

McDermid, S., Nocco, M., Lawston-Parker, P., Keune, J., Pokhrel, Y., Jain, M., Jägermeyr, J., Brocca, L., Massari, C., and Jones, A. D.: Irrigation in the earth system, Nature Reviews Earth & Environment, 4, 435–453, 2023.

Merbold, L., Eugster, W., Stieger, J., Zahniser, M., Nelson, D., and Buchmann, N.: Greenhouse gas budget ($CO_2$, $CH_4$ and $N_2O$) of intensively managed grassland following restoration, Global Change Biology, 20, 1913–1928, 2014.

Mwangi, S., Olioso, A., Etchanchu, J., Mallick, K., Jia, A., Demarty, J., Farhani, N., Sarrazin, E., Gamet, P., and Roujean, J.-L.: Uncertainties in long-term ensemble estimates of contextual evapotranspiration over southern France, Hydrology and Earth System Sciences, 30, 1117–1142, 2026.

Nabuurs, G.-J., Mrabet, R., Abu Hatab, A., Bustamante, M., Clark, H., Havlík, P., House, J., Mbow, C., Ninan, K. N., and Popp, A.: Agriculture, forestry and other land uses (chapter 7), IPCC 2022: Climate Change 2022: Mitigation of Climate Change. Contribution of Working Group III to the Sixth Assessment Report of the Intergovernmental Panel on Climate Change, pp. 747–860, 2023.

Nelson, J. A., Carvalhais, N., Migliavacca, M., Reichstein, M., and Jung, M.: Water-stress-induced breakdown of carbon–water relations: indicators from diurnal FLUXNET patterns, Biogeosciences, 15, 2433–2447, 2018.

Nelson, J. A., Walther, S., Gans, F., Kraft, B., Weber, U., Novick, K., Buchmann, N., Migliavacca, M., Wohlfahrt, G., and Šigut, L.: X-BASE: the first terrestrial carbon and water flux products from an extended data-driven scaling framework, FLUXCOM-X, Biogeosciences, 21, 5079–5115, 2024.

Okujeni, A., van der Linden, S., Tits, L., Somers, B., and Hostert, P.: Support vector regression and synthetically mixed training data for quantifying urban land cover, Remote Sensing of Environment, 137, 184–197, 2013.

Payrosangari, S., Fuchs, K., Wolf, B., Kiese, R., and Scheer, C.: Modelling $N_2O$ emissions in fertilized grasslands with machine learning: a multi-site LSTM approach, EGUsphere, 2025, 1–21, 2025.

Pazúr, R., Huber, N., Weber, D., Ginzler, C., and Price, B.: A national extent map of cropland and grassland for Switzerland based on Sentinel-2 data, Earth System Science Data, 14, 295–305, https://doi.org/10.5194/essd-14-295-2022, 2022.

Phillips, R. L., Tanaka, D. L., Archer, D. W., and Hanson, J. D.: Fertilizer application timing influences greenhouse gas fluxes over a growing season, Journal of Environmental Quality, 38, 1569–1579, 2009.

Poeplau, C. and Don, A.: Carbon sequestration in agricultural soils via cultivation of cover crops–A meta-analysis, Agriculture, Ecosystems & Environment, 200, 33–41, 2015.

Rebmann, C., Aubinet, M., Schmid, H., Arriga, N., Aurela, M., Burba, G., Clement, R., De Ligne, A., Fratini, G., and Gielen, B.: ICOS eddy covariance flux-station site setup: a review, International Agrophysics, 32, 471–494, 2018.

https://doi.org/10.5194/egusphere-2026-3522
Preprint. Discussion started: 26 June 2026


Reinermann, S., Asam, S., and Kuenzer, C.: Remote sensing of grassland production and management—A review, Remote Sensing, 12, 1949, 2020.

Richter, R., Louis, J., and Müller-Wilm, U.: Sentinel-2 MSI–Level 2a products algorithm theoretical basis document, European Space Agency, 49, 1–72, 2012.

Rivera, J. E. and Chará, J.: $CH_4$ and $N_2O$ emissions from cattle excreta: a review of main drivers and mitigation strategies in grazing systems, Frontiers in Sustainable Food Systems, 5, 657 936, 2021.

Rogger, J., Hörtnagl, L., Buchmann, N., and Eugster, W.: Carbon dioxide fluxes of a mountain grassland: drivers, anomalies and annual budgets, Agricultural and Forest Meteorology, 314, 108 801, 2022.

Sabbatini, S., Mammarella, I., Arriga, N., Fratini, G., Graf, A., Hörtnagl, L., Ibrom, A., Longdoz, B., Mauder, M., Merbold, L., et al.: Eddy covariance raw data processing for $CO_2$ and energy fluxes calculation at ICOS ecosystem stations, International Agrophysics, 32, 495–515, 2018.

Saha, D., Basso, B., and Robertson, G. P.: Machine learning improves predictions of agricultural nitrous oxide (N2O) emissions from intensively managed cropping systems, Environmental Research Letters, 16, 024 004, 2021.

Sainte Fare Garnot, V. and Landrieu, L.: Panoptic segmentation of satellite image time series with convolutional temporal attention networks, https://arxiv.org/abs/2107.07933, 2022.

Schwieder, M., Wesemeyer, M., Frantz, D., Pfoch, K., Erasmi, S., Pickert, J., Nendel, C., and Hostert, P.: Mapping grassland mowing events across Germany based on combined Sentinel-2 and Landsat 8 time series, Remote Sensing of Environment, 269, 112 795, 2022.

Sharma, P., Basso, B., Manuraj, A., Murillo, M. S., Millar, N., Tadiello, T., Sharma, M., Delandmeter, M., and Robertson, G. P.: Coupled machine learning–ecosystem ensemble models substantially improve predictions of nitrous oxide ($N_2O$) fluxes from US croplands, Proceedings of the National Academy of Sciences, 123, e2524808 123, 2026.

Smith, W., Grant, B., Desjardins, R., Rochette, P., Drury, C., and Li, C.: Evaluation of two process-based models to estimate soil $N_2O$ emissions in Eastern Canada, Canadian Journal of Soil Science, 88, 251–260, 2008.

Tian, H., Pan, N., Thompson, R. L., Canadell, J. G., Suntharalingam, P., Regnier, P., Davidson, E. A., Prather, M., Ciais, P., Muntean, M., et al.: Global nitrous oxide budget (1980–2020), Earth System Science Data, 16, 2543–2604, 2024.

Tramontana, G., Ichii, K., Camps-Valls, G., Tomelleri, E., and Papale, D.: Uncertainty analysis of gross primary production upscaling using Random Forests, remote sensing and eddy covariance data, Remote Sensing of Environment, 168, 360–373, 2015.

Tschurr, F., Graf, L. V., Walter, A., and Aasen, H.: Enhanced gap-filling for satellite-derived crop monitoring using temperature-driven reconstruction techniques, Smart Agricultural Technology, 10, 100 816, 2025.

Turco, F., Feigenwinter, I., Allemann, J., Hörtnagl, L., Liebisch, F., and Buchmann, N.: fabioturc/n2o-wheat-drivers-sources: version 2025-12-28, https://doi.org/10.5281/zenodo.18075225, 2025.

Turkoglu, M. O., D'Aronco, S., Perich, G., Liebisch, F., Streit, C., Schindler, K., and Wegner, J. D.: Crop mapping from image time series: Deep learning with multi-scale label hierarchies, Remote Sensing of Environment, 264, 112 603, 2021.

Turkoglu, M. O., Ledain, S., and Aasen, H.: Model-agnostic, temperature-informed sampling enhances cross-year crop mapping with deep learning, arXiv preprint arXiv:2506.12885, 2025.

United Nations: World fertility and family planning 2020: Highlights, UN, ISBN 9210043693, 2020.

Wang, Y., Feigenwinter, I., Hörtnagl, L., Gilgen, A. K., and Buchmann, N.: Drivers of long-term grassland $CO_2$ fluxes: effects of management and meteorological conditions during regrowth periods, Biogeosciences, 23, 1625–1652, 2026.

https://doi.org/10.5194/egusphere-2026-3522
Preprint. Discussion started: 26 June 2026


Weber, D., Schwieder, M., Ritter, L., Koch, T., Psomas, A., Huber, N., Ginzler, C., and Boch, S.: Grassland-use intensity maps for Switzerland based on satellite time series: Challenges and opportunities for ecological applications, Remote Sensing in Ecology and Conservation, 10, 312–327, 2024.

Weiss, M. and Baret, F.: S2ToolBox Level 2 Products: LAI, FAPAR, FCOVER, Tech. rep., http://step.esa.int/docs/extra/ATBD_S2ToolBox_L2B_V1.1.pdf, 2016.

Williams, C. A., Reichstein, M., Buchmann, N., Baldocchi, D., Beer, C., Schwalm, C., Wohlfahrt, G., Hasler, N., Bernhofer, C., Foken, T., et al.: Climate and vegetation controls on the surface water balance: synthesis of evapotranspiration measured across a global network of flux towers, Water Resources Research, 48, 2012.

Wu, X., Liu, H., Zheng, X., Lu, F., Wang, S., Li, Z., Liu, G., and Fu, B.: Responses of $CH_4$ and $N_2O$ fluxes to land-use conversion and fertilization in a typical red soil region of southern China, Scientific Reports, 7, 10 571, 2017.

Yang, H., Munson, S. M., Huntingford, C., Carvalhais, N., Knapp, A. K., Li, X., Peñuelas, J., Zscheischler, J., and Chen, A.: The detection and attribution of extreme reductions in vegetation growth across the global land surface, Global Change Biology, 29, 2351–2362, 2023a.

Yang, Y., Roderick, M. L., Guo, H., Miralles, D. G., Zhang, L., Fatichi, S., Luo, X., Zhang, Y., McVicar, T. R., and Tu, Z.: Evapotranspiration on a greening Earth, Nature Reviews Earth & Environment, 4, 626–641, 2023b.

Yang, Y., Tilman, D., Jin, Z., Smith, P., Barrett, C. B., Zhu, Y.-G., Burney, J., D'Odorico, P., Fantke, P., and Fargione, J.: Climate change exacerbates the environmental impacts of agriculture, Science, 385, eadn3747, 2024.

Yin, G., Verger, A., Filella, I., Descals, A., and Peñuelas, J.: Divergent estimates of forest photosynthetic phenology using structural and physiological vegetation indices, Geophysical Research Letters, 47, e2020GL089 167, 2020.

Ying, Q., Poulter, B., Watts, J. D., Arndt, K. A., Virkkala, A.-M., Bruhwiler, L., Oh, Y., Rogers, B. M., Natali, S. M., Sullivan, H., Armstrong, A., Ward, E. J., Schiferl, L. D., Elder, C. D., Peltola, O., Bartsch, A., Desai, A. R., Euskirchen, E., Goeckede, M., Lehner, B., Nilsson, M. B., Peichl, M., Sonnentag, O., Tuittila, E.-S., Sachs, T., Kalhori, A., Ueyama, M., and Zhang, Z.: $WetCH_4$: a machine-learning-based upscaling of methane fluxes of northern wetlands during 2016-2022, Earth System Science Data, 17, 2507–2534, https://doi.org/10.5194/essd-17-2507-2025, 2025.

Yuan, W., Luo, Y., Richardson, A. D., Oren, R. A. M., Luyssaert, S., Janssens, I. A., Ceulemans, R., Zhou, X., Grünwald, T., and Aubinet, M.: Latitudinal patterns of magnitude and interannual variability in net ecosystem exchange regulated by biological and environmental variables, Global Change Biology, 15, 2905–2920, 2009.

Yue, Q., Cheng, K., Ogle, S., Hillier, J., Smith, P., Abdalla, M., Ledo, A., Sun, J., and Pan, G.: Evaluation of four modelling approaches to estimate nitrous oxide emissions in China's cropland, Science of the Total Environment, 652, 1279–1289, 2019.

Zentgraf, I., Holz, M., Monzón Díaz, O. R., Lück, M., Kramp, K., Pusch, V., Grahmann, K., and Hoffmann, M.: How scale affects $N_2O$ emissions in heterogeneous fields of a diversified agricultural landscape, Scientific Reports, 15, 11 013, 2025.

Zhang, H., Deng, Q., Schadt, C. W., Mayes, M. A., Zhang, D., and Hui, D.: Precipitation and nitrogen application stimulate soil nitrous oxide emission, Nutrient Cycling in Agroecosystems, 120, 363–378, 2021.

Zhang, Z., Eddy, W. C., Stuchiner, E. R., DeLucia, E. H., and Yang, W. H.: A conceptual model explaining spatial variation in soil nitrous oxide emissions in agricultural fields, Communications Earth & Environment, 5, 730, https://doi.org/10.1038/s43247-024-01875-w, 2024.

Zhou, W., Rao, P., Jat, M. L., Singh, B., Poonia, S., Bijarniya, D., Kumar, M., Singh, L. K., Schulthess, U., and Singh, R.: Using Sentinel-2 to track field-level tillage practices at regional scales in smallholder systems, Remote Sensing, 13, 5108, 2021.

Zhu, Q., Arndt, K. A., Yuan, K., Li, F., Ying, Q., Liu, L., Ward, E., Malhotra, A., Zheng, J., Yuan, F., et al.: Multi-Decadal Dynamics of Wetland Methane Emissions Revealed by Knowledge-Guided Machine Learning, Global Change Biology, 32, e70 899, 2026.

https://doi.org/10.5194/egusphere-2026-3522
Preprint. Discussion started: 26 June 2026


Zhu, S., Olde, L., Lewis, K., Quaife, T., Cardenas, L., Loick, N., Xu, J., and Hill, T.: Eddy covariance fluxes over managed ecosystems extrapolated to field scales at fine spatial resolutions, Agricultural and Forest Meteorology, 342, 109 675, 2023.